ADVANCED OPTICAL MATERIALS

www.advopticalmat.de

Soft Actuators of Liquid Crystal Polymers Fueled by Light from Ultraviolet to Near Infrared

*Lang Qin, Xiaojun Liu, and Yanlei Yu**

Photodeformable liquid crystal polymers (LCPs) are a typical representative of shape-changing systems capable of remotely converting light energy into mechanical actuation. Such smart polymeric materials combining the features of polymers and liquid crystals (LCs) are envisioned to bring new functionality and drive innovation in the fields of soft robotics, solar-energy harvesting, and microfluidics. The photodeformable LCPs and their soft actuators fueled by light from ultraviolet to near infrared, including basic actuation as well as the primary mechanisms are focused on. The complex actuation is also highlighted with emphasis on the designed LC alignment, such as splayed, twisted, out-plane, and patterned, which bridges the gap between the shape change and practical applications. Special attention is devoted to the progress of light-fueled soft actuators, which are classified into different categories and comprehensively summarized in the aspects of materials, alignment, mechanisms, and light stimuli. An outlook on future challenges and limitations in the light-fueled soft actuators are discussed at the end of this review.

1. Introduction

An area where nature widely arouses interests is that of active, stimuli-responsive, and shape-changing materials. This biological intelligence has inspired a new class of smart polymeric materials, which respond to external stimuli by changing shapes.[1] Polymeric materials exhibiting liquid crystallinity are a typical representative of these smart systems, which combine the features of polymers and liquid crystal (LC) materials, such as elasticity, anisotropy, self-assembly, and intermolecular cooperative effect.[2] LC polymers (LCPs) used in shape-changing systems can be referred to crosslinked liquid crystal polymers (CLCPs), including liquid crystal polymer networks (LCNs) and liquid crystal elastomers (LCEs), and linear liquid crystal polymers (LLCPs) (**Figure 1**a). LCNs contain a moderate to densely crosslinked network, whereas LCEs typically consist of the flexible backbone and overall crosslink density is low.[3] Such deformable materials have been considered as a promising candidate for artificial muscles and demonstrated versatile potential applications in soft actuators.[4]

Dr. L. Qin, X. Liu, Prof. Y. Yu
Department of Materials Science and State Key Laboratory of Molecular Engineering of Polymers
Fudan University
Shanghai 200433, China
E-mail: ylyu@fudan.edu.cn

The ORCID identification number(s) for the author(s) of this article can be found under https://doi.org/10.1002/adom.202001743.

DOI: 10.1002/adom.202001743

Various stimuli have been implemented to trigger deformation of the LCPs. Compared to other stimuli, such as by heat, magnetic fields, acoustic waves, pressure, pH variation, humidity, and electricity, light stimulus is ideal because it enables remote and noncontact manipulation and can be conveniently and precisely tuned in terms of intensity, wavelength, and polarization.[5] Therefore, photodeformable LCPs are capable of converting light energy into mechanical actuation (shape change) activated by photochemical or/and photothermal effect with the aid of photosensitive units in the materials.[6] In the past decades, light with different polarization, patterns, and wavelengths from ultraviolet (UV) to near infrared (NIR) has been employed to trigger the shape change of the LCPs owing to the innovation of materials.[7] An increasing number of remarkable results have been reported in light-fueled soft actuators of the LCPs and complex devices also have been ingeniously designed on the basis of distinct LC alignment that determines the actuation modes.

In this review, we mainly introduce the photoinduced deformation of the LCPs based on photochemical and photothermal effect by taking the wavelength of the light stimuli as the clue. The basic actuation as well as primary mechanisms is presented, followed by a description of complex actuation determined by the designed LC alignment. We summarize the light-fueled soft actuators according to the concept of locomotion, oscillation, self-sustainable motion, self-regulation, and liquid manipulation. Within this framework, we provide an outlook for the development of photodeformable LCPs in the near future.

2. Basic Actuation: Contraction and Bending

In 1975, de Gennes theoretically proposed the possibility to induce the macroscopic deformation of CLCPs through the significant change in the alignment of mesogens (order degree) by external stimulus.[8] The fundamental principle of the reversible deformation lies in the conformational change of the polymer backbone upon the order–disorder alignment change (Figure 1b). The conformation of polymer chains closely relates to the macroscopic shape, and is strongly coupled with the alignment of mesogens, which can be altered by light stimuli according to three major mechanisms, including photochemical phase transition, photoreorientation, and photothermal effect (Figure 1c). In this section, we summarize the light stimuli with

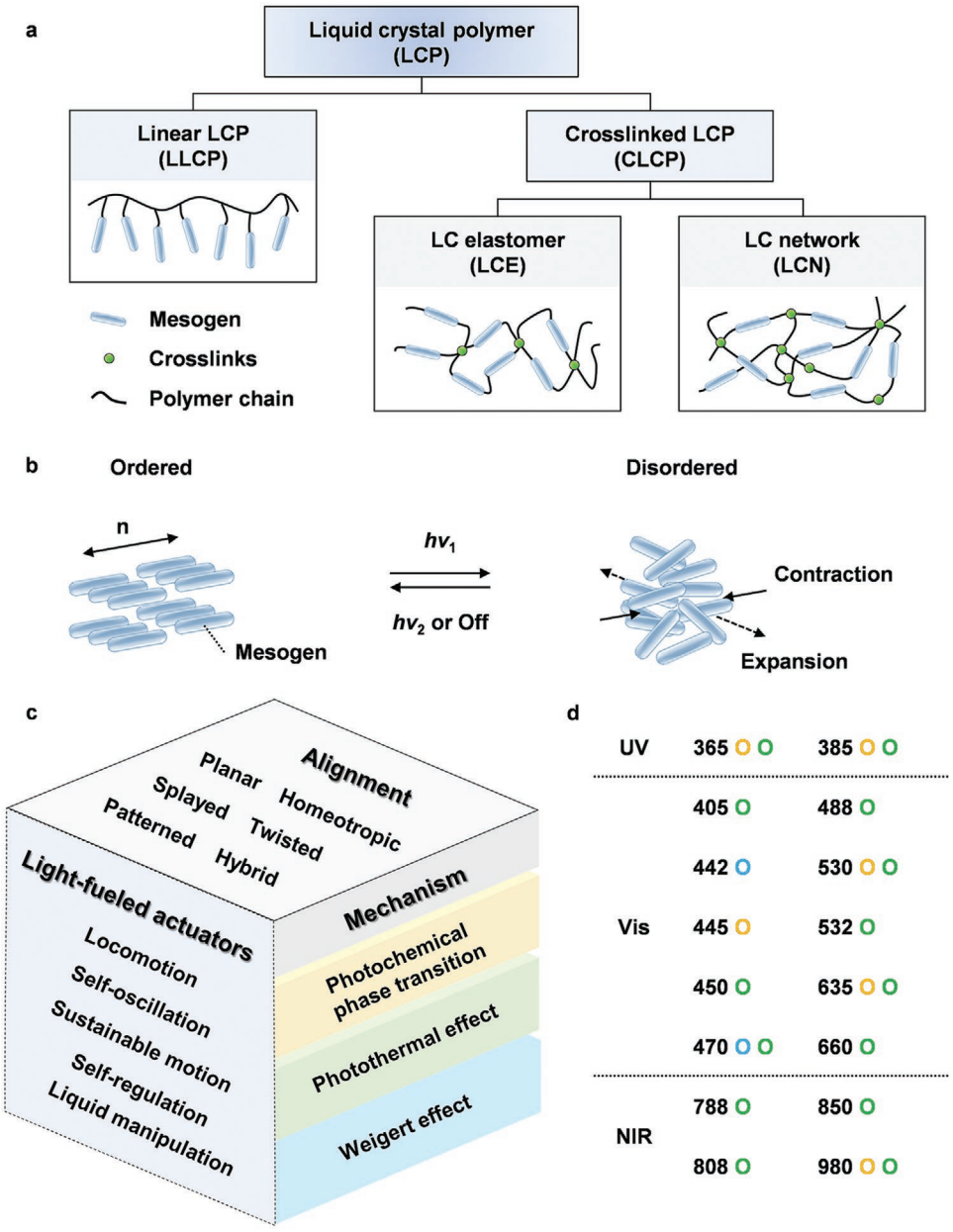

Figure 1. a) Classification of the general photodeformable LCPs. b) Schematic illustration to show the basic mechanism behind the shape change of the LCPs. c) Three major mechanisms for photodeformation of the LCPs and different light-fueled actuation for applications. d) Summary of the wavelength and their corresponding mechanisms of the commonly used light stimuli from UV to NIR. Orange circle, photochemical phase transition; blue circle, Weigert effect (photoreorientation); green circle, photothermal effect.

different wavelengths used to induce the deformation of CLCPs (Figure 1d) and will discuss the basic contraction and bending actuation based on three classical mechanisms induced by light from UV to NIR as well as the corresponding material systems.

2.1. Photochemical Phase Transition Triggered by Light with Different Wavelengths

The study of photochemical phase transition in LCPs started with the incorporation of azobenzene moiety, which is a well-known chromophore that can serve as both the photo-responsive group and the mesogen.[9] The most interesting property of azobenzene molecules is the fact that the switch between the two isomers can be triggered by the absorption of different photons efficiently and repeatedly. The UV light irradiation causes the switch of azobenzene molecules from the energetically favored *trans*-state to the *cis*-state, which then recovers to the *trans*-state either by blue/green light irradiation or by thermal relaxation.[2c,10] The rod-like *trans* isomer of the azobenzene stabilizes the phase structure of the LC, whereas its bent *cis* isomer tends to destroy the LC alignment. When

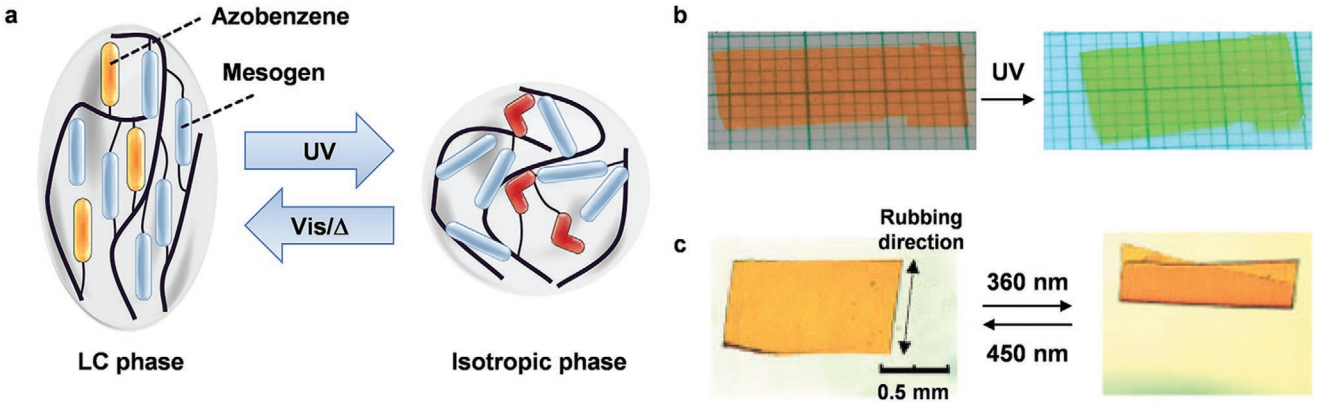

Figure 2. a) Schematic illustration to show the deformation based on reversible LC-isotropic photochemical phase transition. b) Photographs to show photoinduced contraction of the LCE before UV irradiation (left) and under UV irradiation (irradiation time: 130 s, right). Reproduced with permission.[12] Copyright 2003, Wiley-VCH. c) Bending and unbending behavior of the LC gel film in toluene. The LC gel film bent toward the irradiation direction of UV light (360 nm) and reverted to the initial flat film completely upon irradiation of visible light (450 nm). Reproduced with permission.[13a] Copyright 2003, Wiley-VCH.

photochromic azobenzene moieties are covalently bonded into the polymer network, the phase transition from the ordered LC phase to disordered isotropic phase is induced isothermally by the conformational change of azobenzenes upon light irradiation, which eventually lead to a macroscopic deformation of the entire crosslinked network because of the cooperative effect (**Figure 2**a). This phenomenon known as cooperative effect illustrates that the energy required to change the alignment of only 1 mol% LC molecules is enough to change the alignment of the whole system.

Finkelmann et al. reported the pioneering work on photoinduced deformation of a monodomain nematic CLCP consisting of a polysiloxane main chain and azobenzene chromophores at crosslinks.[11] They predicted that the CLCP could generate shape change between 10% and 400% upon irradiation, and succeed in demonstrating photoinduced uniaxial contraction along the LC alignment by 20% upon UV irradiation. This work indicates the significant reversible deformation of CLCPs based on photochemical phase transition, where the photomechanical effect is necessary to be taken into consideration. Keller and co-workers endeavored to synthesize monodomain side-on azobenzene-containing CLCPs by photopolymerization with a NIR photoinitiator.[12] Compared to the end-on structure, the side-on systems possess a stronger chain anisotropy because of the enhanced coupling between the backbone and mesogens. The obtained thin film was found to show fast (<1 min) contraction of up to 18% upon UV irradiation at 70 °C (Figure 2b), which greatly improved the response speed of photoinduced CLCPs.

In addition to contraction and expansion, a 3D bending mode of azobenzene-containing monodomain CLCP gels, films and fibers was reported by Ikeda et al. for the first time.[13] The CLCP films bent toward the light source along the direction of the mesogen alignment upon 366 nm UV irradiation and reverted to the initial flat state when exposed to 450 nm light (Figure 2c). Due to the high extinction coefficient of the azobenzene, more than 99% incident photons were absorbed by the surface region with a thickness less than 1 μm. Thus, the light absorbance within the film was no longer constant, and the efficiency of photoisomerization varied throughout the direction of thickness. The contraction was locally induced near the surface, which generated internal stress that leads to bending of the whole film.

To acquire high-speed deformation at room temperature, Ikeda and co-workers prepared ferroelectric LCE films with high degree of order of mesogens.[14] The bending process was completed upon exposure to a laser beam in 500 ms, which is one order of magnitude faster than that of the nematic films. Notably, the photoinduced mechanical force (about 220 kPa) is similar to the contraction force of human muscles. Following the preliminary researches, numerous efforts have been made to investigate the effects of the crosslinking density,[15] the spacer length of the monomer and crosslinker,[16] concentration of photoactive chromophores,[17] and the location of azobenzenes[18] on the bending deformation of the LCPs.

Inspired by the concerted motion of cilia in the respiratory system to transport species over a static surface, Broer and co-workers reported the movement of objects in a liquid induced by the cooperative bending motion of the azobenzene-based main-chain CLCP fiber arrays.[19] The fibers (length: 10–15 mm, diameter: 70 μm) with high degree of alignment were obtained by drawing the main chain LC oligomers with a suitable viscosity in nematic phase, followed by crosslinking with photoresponsive azobenzene monomer. Initiated by gradient photochemical phase transition from the exposed side inward, the fibers bend simultaneously toward the 365 nm UV light (25 mW cm^{-2}). Moreover, the fibers demonstrated sunflower-like light-tracking movements by adjusting the bending direction follow the UV light in all directions, which was ascribed to the fast transformation between *trans* and *cis* isomer. To mimic the natural cilia's motion to transport species, an asymmetric motion of the fiber arrays including an effective stroke and a recovery stoke was designed. The initially straight fibers array immersed in paraffin oil (37 °C) firstly bend forward UV light at an angle of 48° ± 7°, then rotate 90° horizontally follow the light, and finally recover to the initial straight state when the light is placed above. In this process, the collective asymmetric bending induces the floating plastic flakes (200 μm thick and

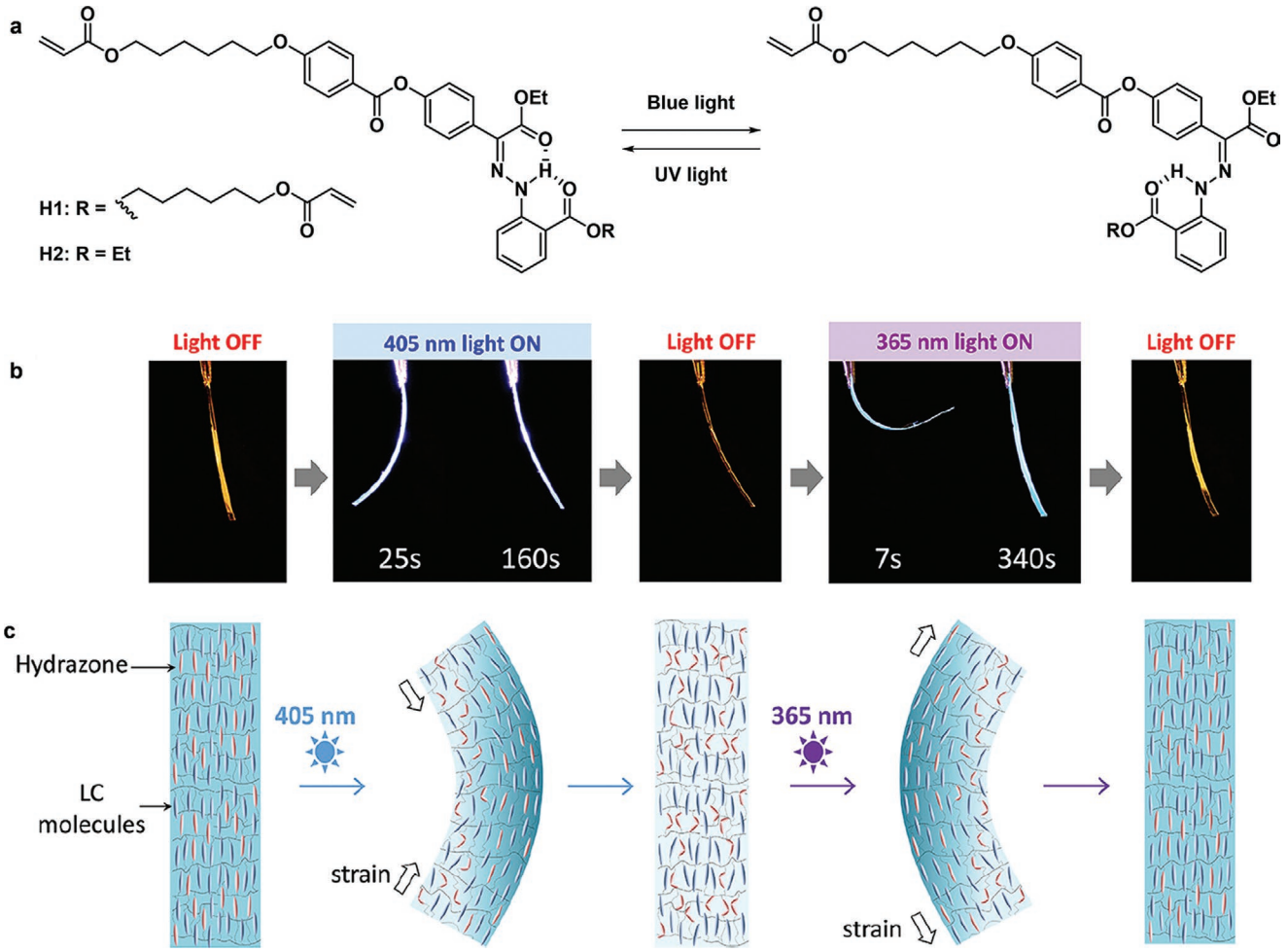

Figure 3. a) Chemical structures of hydrazones H1 and H2. b) Photoactuation of the polymer ribbons incorporating H1. Thickness, 25 µm. c) Representation of the photoinduced shape-shifting. Reproduced with permission.[21] Copyright 2019, American Chemical Society.

1 mm^2 size) to move forward. Furthermore, Schenning, Broer, and co-workers demonstrated the light guiding behavior of the fiber arrays by integrating them with a red emitting fluorescent dye-doped polymethyl methacrylate plate, where the refractive indices of the fibers and the plate are matched.[20] The behavior of the fibers to track a light source and guide the collected light, making these responsive actuator arrays potentially attractive for advanced photovoltaic and optical elements.

Azobenzenes have been widely used in photoresponsive LCPs, however, most of azobenzene-based actuators lack photoinduced shape stability, because the *cis* isomer is transient under dark. Recently, Katsonis, Aprahamian, and co-workers reported on a photoresponsive LCN with negatively photochromic hydrazones as photochemical switches, which was used to create a large range of shapes with a long-term stability (**Figure 3**a).[21] The major contribution in shape transformation originates from mechanical stresses generated by the photoisomerization of hydrazones. Upon 405 nm light irradiation, the planar aligned polymer ribbon bends toward the light, because only the switches in the irradiated surface undergo *Z*–*E* isomerization, causing a gradient mechanical stress. Further irradiation leads to the isomerization of the negatively photochromic hydrazones throughout the entire thickness of the polymer ribbon, inducing that the ribbon bends back to its original shape. Subsequent irradiation with 365 nm UV light results in an opposite process due to the gradual conversion of *E*-isomer into the *Z*-isomer (Figure 3b,c). The stability of both the *Z*- and *E*-forms allows fixing any isomeric composition. As a result, the photoinduced shapes are stable for months.

To exploit potential applications of photoinduced actuators in biological systems, low energy light, compared to UV light, is preferred because low energy light causes less damage to biosamples and penetrates deeper into tissues. It would be attractive to develop the LCP systems that undergo shape change in response to visible and NIR light, or even sunlight. The visible-light-induced bending of azotolane-containing CLCPs was firstly reported by Yu and co-workers, which even deformed upon irradiation with sunlight.[22] Compared to the absorption at 366 nm of normal azobenzenes, a decrease of energy level difference in the π–π^* leads to that the maximum absorption in the azotolane red-shifts to 385 nm (**Figure 4**a). Irradiated with 436 nm visible light, the film bent toward the irradiation direction of the light due to the *trans-cis* photoisomerization of azotolane and reverted to the initial state upon exposure to 577 nm visible

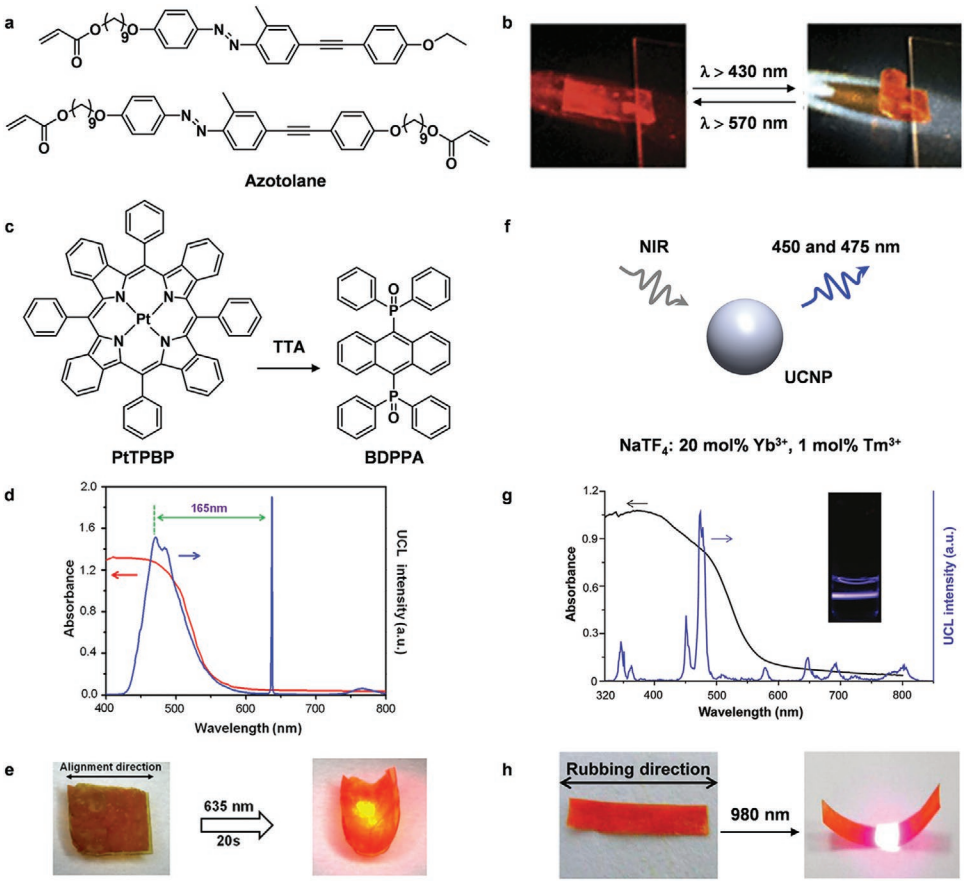

Figure 4. a) Examples of chemical structures of the monomer and crosslinker containing azotolane moieties used to prepare the visible-light-driven CLCP films. b) Photoinduced bending and unbending motion of the azotolane-containing CLCP film in sunlight through a lens and glass filters. The sunlight at >430 and at >570 nm is acquired by using different filters. Reproduced with permission.[23] Copyright 2009, The Royal Society of Chemistry. c) Chemical structures of PtTPBP (sensitizer) and BDPPA (annihilator). d) UCL emission spectrum (blue line) of the toluene solution of PtTPBP&BDPPA (λ_{ex} = 635 nm, power density = 200 mW cm^{-2}) and the UV–vis absorption spectrum (red line) of the azotolane CLCP film. e) Photographs of the as-prepared assembly film bending toward the light source along the alignment direction of the mesogens in response to the 635 nm laser with the power density of 200 mW cm^{-2}. Reproduced with permission.[25] Copyright 2013, American Chemical Society. f) UCNPs composed of $NaYF_4$: 20 mol% Yb^{3+}, 1 mol%Tm^{3+}. g) UCL emission spectrum (blue line) of a colloidal $CHCl_3$ solution of UCNPs (1 mg mL^{-1}) excited with a 980 nm CW laser (power = 600 mW, power density = 15 W cm^{-2}) and the UV–vis absorption spectrum (black line) of the azotolane CLCP film. h) Photographs of the azotolane CLCP/UCNP composite film bending toward the light source along the alignment direction of the mesogens in response to the CW NIR irradiation at 980 nm (power density = 15 W cm^{-2}). Reproduced with permission.[26] Copyright 2011, American Chemical Society.

light. Interestingly, the azotolane-containing CLCP film also underwent sunlight-induced bending and unbending by tuning the wavelength through a lens (Figure 4b).[23] Such sunlight-responsive films are significant in the development of solar energy harvest because they directly convert endlessly supplied solar energy into mechanical work. By using this material, they prepared a fully plastic microrobot driven by visible light.[24] The microrobot consisted of several units made of the CLCP/polyethylene bilayer film, including a hand, a wrist, and an arm. Without the aid of any gears, bearings, or contact-based driving systems, the microrobot was remotely manipulated to pick, lift, move, and even place the milligram-scale object by irradiating different units with blue light.

Yu, Li, and co-workers extended the wavelength of light stimulus to 635 nm and achieved the red-light-induced deformation of a composite film triggered by low-powered excited upconversion luminescence (UCL) on the basis of triplet–triplet annihilation (TTA).[25] The TTA-based UCL has several advantages, such as high quantum efficiency, large anti-Stokes shift, and low excitation power density. Platinum(II) tetraphenyltetrabenzoporphyrin (PtTPBP) and 9,10-bis(diphenylphosphoryl)anthracene (BDPPA) were incorporated into a rubbery polyurethane film as the sensitizer and the annihilator, which was assembled with the azotolane-containing CLCP film (Figure 4c). Upon exposure to 635 nm red light, the PtTPBP&BDPPA-containing polyurethane film trapped the incident light like an antenna and upconverted it into the blue emission (Figure 4d). The UCL emission was subsequently absorbed by the azotolane moieties in the CLCP film via emission–reabsorption process, which induced the bending of the composite film because of *trans–cis* photoisomerization and alignment change of the mesogens (Figure 4e). Surprisingly, even though a piece of 3 mm thick pork was put between the red light and the composite film, the composite film still bent toward the light source. This work proposes a new manner to construct photonic devices by using photodeformable soft materials with the TTA-based

upconversion system. They further demonstrated fast bending of the composite film upon exposure to continuous-wave (CW) NIR light at 980 nm by incorporating upconversion nanophosphors (UCNPs) $NaYF_4$:Yb^{3+},Tm^{3+} into the azotolane-containing CLCP film (Figure 4f).[26] Under excitation with the CW 980 nm laser, the main UCL emission peaks of the UCNPs located at 450 and 475 nm, overlapping the absorption band of the azotolane CLCP film perfectly (between 320 and 550 nm) (Figure 4g). Similarly, the UCL of the nanophosphors not only triggered *trans–cis* photoisomerization, but also led to the alignment change of the mesogens (Figure 4h). 980 nm is the longest wavelength of the light used to induce the deformation of the CLCPs based on photochemical phase transition so far.

2.2. Actuation Triggered by Light with Different Polarization

In addition to the wavelength, polarization is also an important parameter for light stimuli employed to manipulate the photodeformation of the LCPs. Ikeda and co-workers proposed an ingenious strategy to precisely control the bending direction of a polydomain CLCP film by changing the linear polarization direction of incident UV light.[27] The polydomain CLCP films were composed of numerous microscale domains, where azobenzene moieties were randomly aligned in different direction. The linear polarized light was preferentially absorbed by the azobenzene moieties that were aligned in the specific domains along the direction of the light polarization. By means of selective absorption, the polydomain CLCP film bent repeatedly along any chosen direction that was parallel to the polarization of the 366 nm UV light, and completely recovered upon exposure to >540 nm visible light (**Figure 5**).

In typical azobenzene molecular systems, the absorption resonances to induce the *trans–cis* and the *cis–trans* isomerization transitions are broad and significantly overlapped. Even monochromatic photons, typically with wavelength of 400–550 nm, can activate both the photoisomerization reactions efficiently at the same time. As a result, continuously irradiated azobenzene molecules undergo repeated *trans–cis–trans* photoisomerization cycles, which induce the stochastic photoreorientation of the azobenzene molecules exposed to linearly polarized light. This photoreorientation (also known as Weigert effect) originates from the more efficient isomerization dynamics for the azobenzene molecules excited with light polarized along the direction of transition dipole, which is oriented along the molecular main axis of the *trans* isomer.[28] After many photoisomerization cycles, the excited azobenzene molecules become randomly oriented in the direction perpendicular to the light polarization direction and does not absorb photons efficiently anymore even if the light irradiation continues (**Figure 6**a). Tabiryan et al. reported a CLCP film in fast mechanical response to the laser beam with different polarization.[29] The direction of the bending or twisting was reversed by changing the polarization of the laser beam. When the mesogen alignment is perpendicular to the beam polarization (E⊥n), the CLCP film bent away from the laser. Conversely, the CLCP film bent toward the laser when the mesogen alignment is parallel to the beam polarization (E∥n). The film orientation could be varied within ±70°, which was attributed to the reorientation of azobenzene moieties in the CLCP film caused by linearly polarized light.

In the case of the unpolarized light, only the propagation direction of light is always perpendicular to its electric field vector.[30] The azobenzene moieties tend to be aligned only in the propagation direction of the actinic light (Figure 6b). Recently, Yu and co-workers developed a new class of linear LCPs (LLCPs), including homopolymers and copolymers (**Figure 7**a,b), whose deformation was triggered

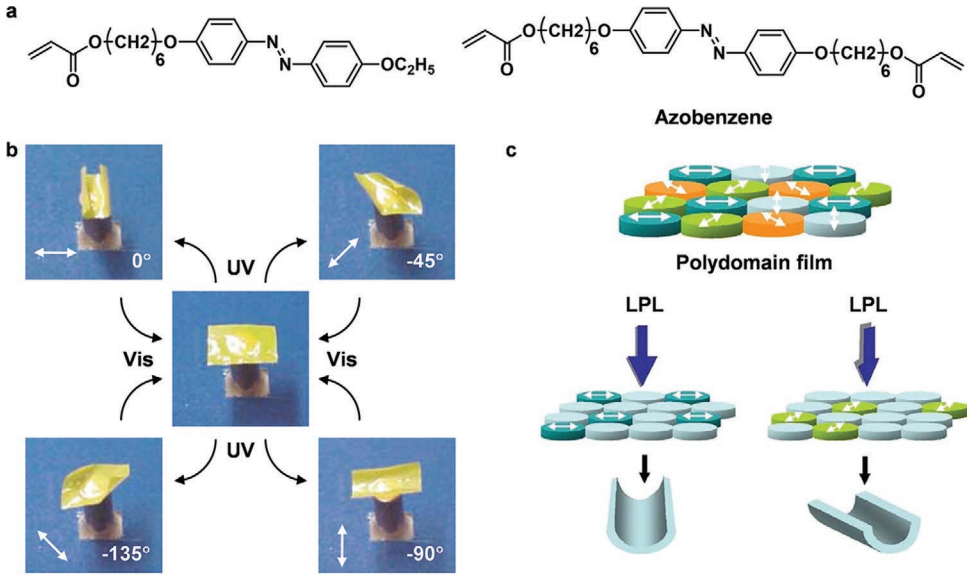

Figure 5. a) Chemical structures of the monomer and crosslinker containing azobenzene moieties used to prepare the CLCP films. b) Photographic frames of the film bending in different directions in response to irradiation by linearly polarized light of different angles of polarization (white arrows) at 366 nm, and being flattened again by visible light longer than 540 nm. Reproduced with permission.[27] Copyright 2003, Springer Nature. c) Schematic illustration of the plausible bending mechanism. LPL, linear polarized light.

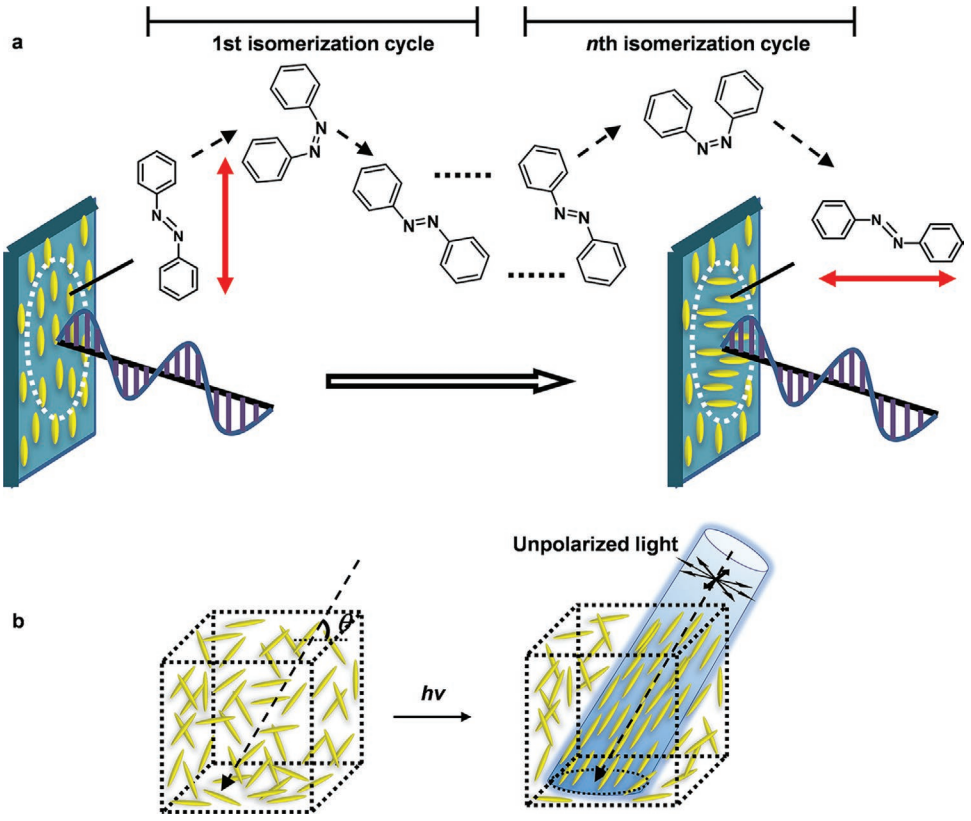

Figure 6. a) Schematic illustration of the photoalignment process of the azobenzene irradiated by linearly polarized light. The direction of molecular alignment is determined by the direction of the electric vector *E* (red arrows) in the irradiating optical field. b) Schematics showing reorientation of mesogens in azobenzene-containing LC systems with nonpolarized light that is incident at angle *θ*. Double arrows show the polarization direction of the light. Reproduced with permission.[30] Copyright 2016, Springer Nature.

by unpolarized light according to Weigert effect.[30,31] The critical design premise of the LLCPs includes ensuring enough mechanical robustness without chemical crosslinks, and realizing macroscopic LC orientation in an easy manner. Inspired by the lamellar structure of artery walls that are natural tough bioactuators, the LLCPs were designed to possess a long alkyl backbone containing double bonds, azobenzene moieties as well as other mesogens in side chains, and spacers with appropriate length. In order to enhance the mechanical robustness, ring-opening metathesis polymerization was employed to prepare the LLCP with high molecular weight. These LLCPs, serving as bulk or partial photoresponsive blocks, were processed into complex tubular actuators with various shapes by conventional methods (melting and solution processing) because of the linear structure (Figure 7c,d). Importantly, highly ordered smectic phase of these LLCPs is facilely obtained by annealing, which is ascribed to the self-assemble ability of the mesogens (Figure 7e). When the tubular actuators were exposed to unpolarized 470 nm light whose actinic direction is perpendicular to the long axis of the actuators, the azobenzene mesogens were reorientated along the propagation direction of the light. The orange and blue parts in the cross-sectional area expanded and contracted along the *y* axis upon light irradiation, respectively (Figure 7f). The photoreorientation decreased the wall thickness and increased the perimeter, which caused an increase of the cross-sectional area.

2.3. Actuation Triggered by Photothermal Effect

Once heated above the LC-isotropic transition temperature, the oriented mesogens will become randomly aligned and bring polymer chains back to the random coil conformation. Accompanying the LC-isotropic phase transition, the LCP contracts along the direction of the original alignment but expands in the perpendicular direction.[32] The thermal-responsive LCP can be readily transformed into photoresponsive one on the basis of photothermal effect. To achieve efficient photothermal-driven deformation, in principle, LCPs are loaded with certain photothermal agents.[33] These agents convert incident light into thermal energy by releasing heat into the LCP matrix, which results in the LC-isotropic phase transition and reversible macroscopic shape change at the same time (**Figure 8**a). Chen, Gong, and coworkers reported that the LCE nanocomposite film loaded with single-walled carbon nanotubes (SWNTs) as the photothermal agent contracted to 80% of its peak shrinkage.[34] Besides carbon nanotubes, a variety of photothermal agents, often in the form of nanofillers, can be selected by taking into consideration a number of general issues, including absorption wavelengths, quantum yield of optical–thermal energy conversion, and dispersity in the LCP matrices.[33a] In this section, we will briefly introduce photothermal-induced deformation of the LCPs.

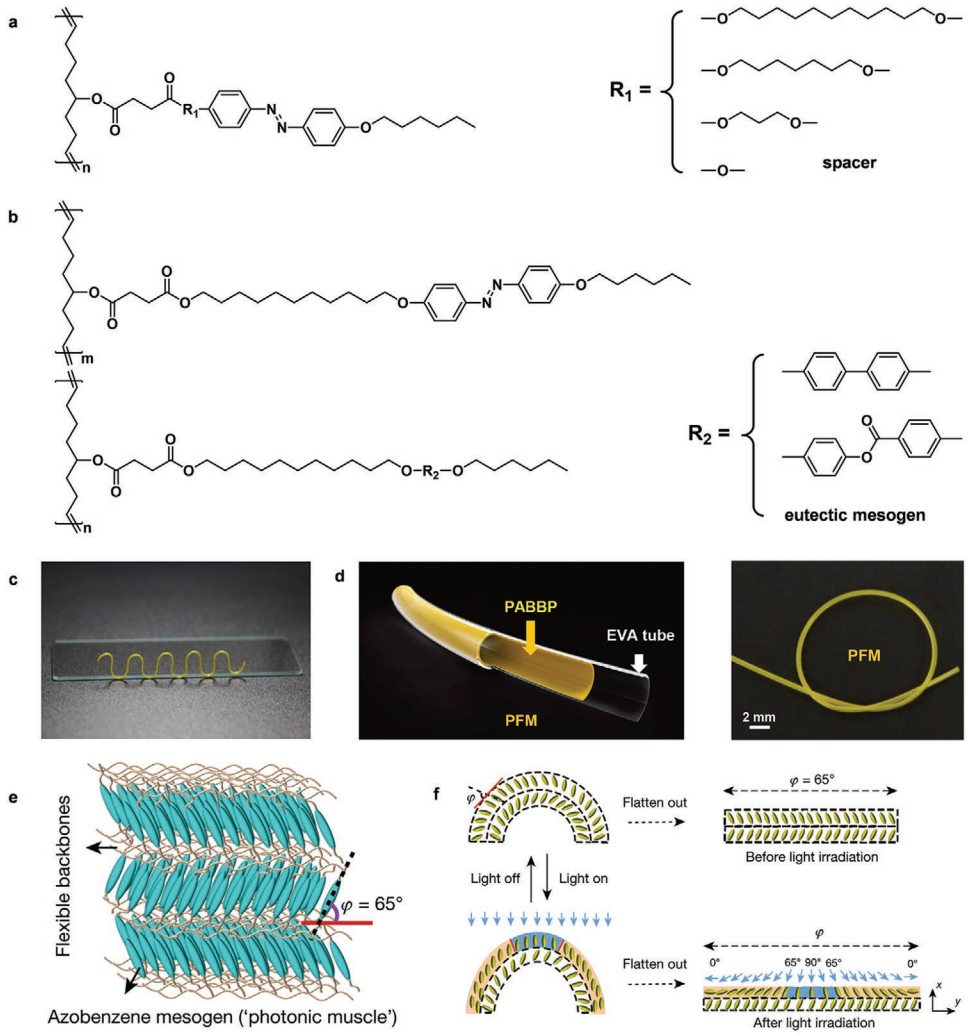

Figure 7. a) Chemical structures of linear liquid crystal homopolymers with different spacer lengths. b) Chemical structures of linear liquid crystal copolymers with different eutectic mesogens. c) A photograph showing a serpentine tubular microactuators (TMA). The serpentine TMA is leaning against the edge of a glass slide. d) Schematic representation of the bilayer structure of the photocontrollable flexible microtube (PFM) and a photograph of a knotted PFM showing good flexibility. Scale bar, 2 mm. Reproduced with permission.[31a] Copyright 2019, Wiley-VCH. e) Schematic representation of packing structure in the LLCP film. The LC mesogens self-assemble into a smectic phase, and the zigzag tilting of LC mesogens takes place in smectic lamella. φ denotes the tilt angle between the long axis of the azobenzene mesogens and the plane of the lamella. f) Schematics illustrating the reorientation of mesogens in the cross-sectional area of the TMA before and after irradiation by unpolarized 470 nm light. This photoinduced reorientation leads to the decrease in thickness of the TMA wall (along the *x* axis) and the elongation of the perimeter of the TMA (along the *y* axis), which contributes to the increase of cross-sectional area. Reproduced with permission.[30] Copyright 2016, Springer Nature.

Broer, Schenning, and co-workers reported a splay-aligned LCN film, which generated various shapes upon light irradiation of different wavelengths.[35] The LCN film contains a pH-sensitive azomerocyanine (AM) dye that can be locally converted to the hydroxyazopyridinium (HAP) form by an acid (Figure 8b). These two derivatives are sensitive to light irradiation of different wavelength and exhibit excellent stability over time. It is noted that the maximum absorption of azomerocyanine located at 550 nm blueshifts to 405 nm of hydroxyazopyridinium after protonation. Therefore, the azomerocyanine-containing film bent strongly (50°) upon exposure to 530 nm light, while the hydroxyazopyridinium form was triggered by 405 nm light. The *trans–cis* photoisomerization and photothermal effect reduced the order in the LCN, leading to anisotropic shape changes. Upon switching off the light, all films unbent immediately. The temperature of the film significantly increased when exposed to light, suggesting that photothermal processes are the dominant factor in the deformation response. Based on locally acid treatment, a film (2.5 cm × 0.4 cm) with three strips of hydroxyazopyridinium regions (405 nm) and four stripes of azomerocyanine regions (530 nm) were made (Figure 8c). When exposed to 405 nm light, only the hydroxyazopyridinium regions (yellow) bend while the purple parts remain straight, vice versa, so that the folding can be controlled by different wavelengths of light in a film. Moreover, the acidic patterning allows to be erased with base and new patterns can be reprogrammed, which gives access to create reusable, adjustable soft actuators.

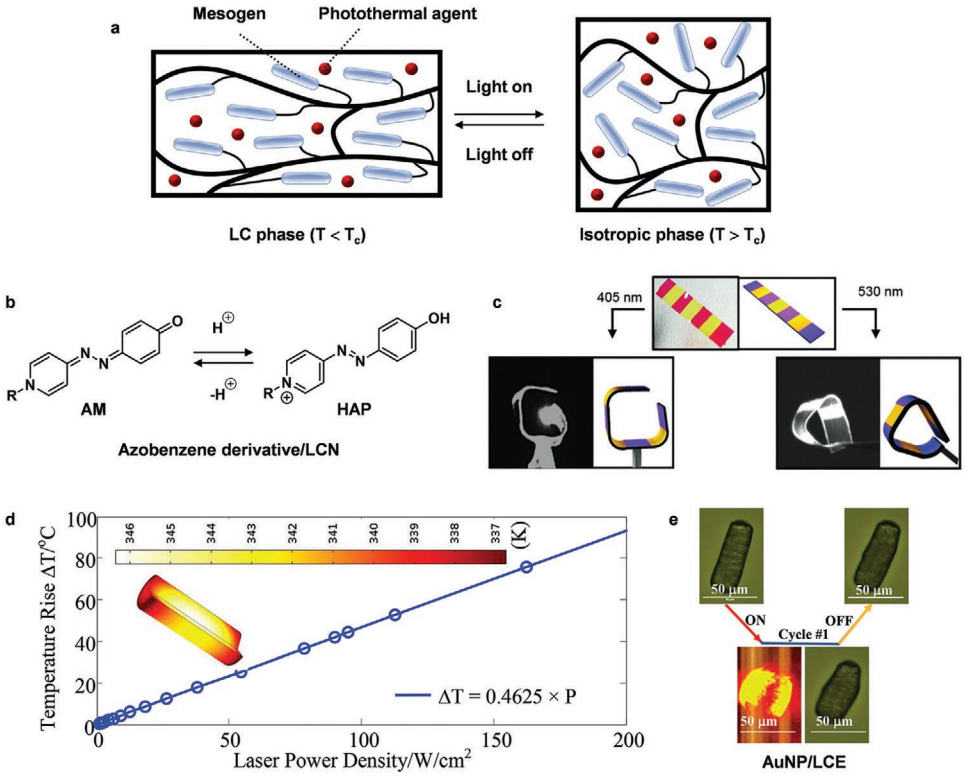

Figure 8. a) Schematic illustration to show the deformation based on the photothermal effect. b) Molecular changes of the azobenzene derivative upon acid and base treatment. c) Specific bending of a patterned film. The same film is exposed with 405 nm (left) and 530 nm (right) light. The film specifically bends at the yellow region when exposed to 405 nm and at the magenta region when exposed with 530 nm. When switching off the light, the film unbends to the flat state. At the right of each image a schematic of the patterned film and its bending behavior is shown. Reproduced with permission.[35] Copyright 2017, Wiley-VCH. d) Finite elemental analysis (FEA) results on the temperature rise of an LCE/AuNR (1 wt%) micropillar (length = 72.2 μm and diameter = 24.6 μm) upon laser irradiation at varied power density. The inset shows the absolute temperature distribution (unit: Kelvin) of the pillar irradiated by 95 W cm^{-2} at an ambient temperature of 298.15 K. e) The snapshots of 635 nm laser irradiation (95 W cm^{-2}) induced shape change for an LCE/AuNR (1 wt%) pillar at 80 °C. Reproduced with permission.[38] Copyright 2015, Wiley-VCH.

In addition to azobenzene derivatives, Priimagi, Zeng, and co-workers reported a photothermal-driven LCN with diarylethene as crosslinker, which undergoes interconversion between open- and closed-form.[36] The LCN film with twisted molecular alignment bent at an angle about 20° when exposed to both UV and visible light simultaneously. It is noted that 365 nm UV light (50 mW cm^{-2}) triggers the conversion of diarylethene from open- to closed-form, and the deformation is ascribed to the photothermal effect of the closed-form diarylethene driven by 550 nm visible light (285 mW cm^{-2}), subsequently triggering the actuation of the LCN.

Overcrowded alkene molecular motors, as one of the most promising photoactive molecules, have also been reported by Yang and co-workers to serve as the photothermal agents incorporated into a LCN.[37] Upon irradiation of UV light (80 mW cm^{-2}), the motor fastened to the polymer chains transferred the light energy into heat rather than triggering photoisomerization, which was sufficient to induce anisotropic deformation of the splayed-aligned LCN film. When the light irradiation ceased, the LCN film recovered fast to the initial shape due to the sharply temperature decrease.

There is recently an emergence on using nanoparticles to form LCE nanocomposites or nanohybrids to activate their shape change based on photothermal effects. The unique localized surface plasmon resonance enhanced photothermal effect of gold nanoparticles makes them especially interesting in developing multifunctional LCE composites with remote triggering capability. Keller, Liu, Wang, and co-workers reported the first-of-a-kind study on the synthesis and fabrication of gold nanosphere and gold nanorod enabled LCE micropillars and their photothermal actuation behavior upon visible laser irradiation.[38] The gold nanorod is a better photothermal agent than gold nanosphere due to the order-enhancement ability originating from the shape anisotropy and higher temperature rise induced by photothermal conversion. Under irradiation of 635 nm light (95 W cm^{-2}), the temperature rise of the LCE/gold nanorod micropillar is 44.2 °C (Figure 8d). To perform the photothermal actuation, where the nematic–isotropic phase transition temperature of the LCE with gold nanorod is 100 °C, the micropillar was suspended in 80 °C silicone oil. When the laser irradiation was switched on, the uniaxially aligned micropillar immediately started to shrink in length and expand in diameter within 5 s. Upon switching off the laser irradiation, the micropillar quickly recovered to its original shape within less than 1.5 s (Figure 8e).

Compared to UV or visible light, long-wavelength NIR light could efficiently penetrate through biomaterials. However, inorganic nanoparticles sensitive to NIR light are difficult to

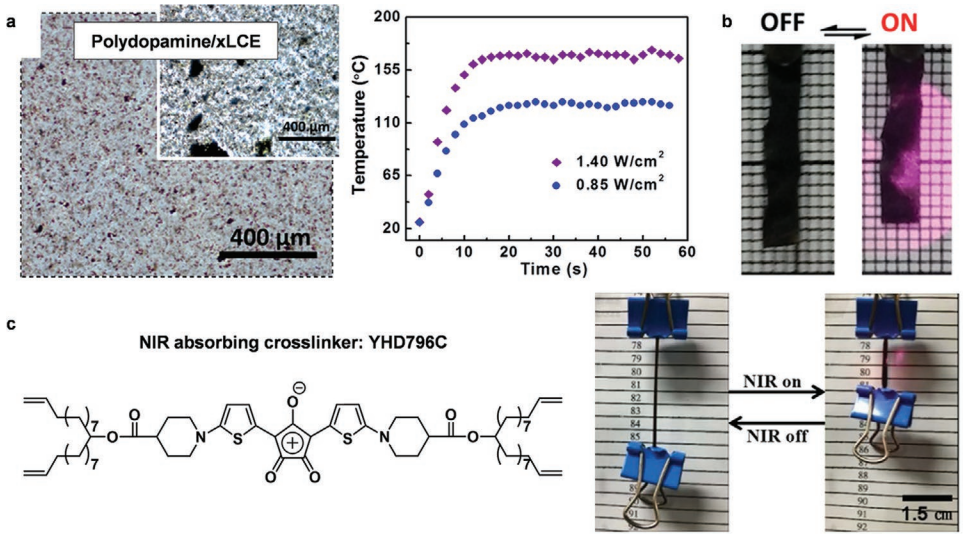

Figure 9. a) Optical micrographs of the PDA-*x*LCE (2 wt%) and CNT-*x*LCE (inset, 0.1 wt%) films in transmission mode (left) and local temperature as a function of irradiation time of a PDA-*x*LCE film under IR irradiation with two different power densities (right). b) Photoactuation of a monodomain PDA-*x*LCE sample under irradiation with an 808 nm wavelength laser. Light intensity: 1.0 W cm^{-2}. Reproduced with permission.[39] Copyright 2017, The Royal Society of Chemistry. c) Chemical structure of the NIR absorbing crosslinker and photographs of an LCE ribbon before and after NIR (808 nm) illumination. Reproduced with permission.[40] Copyright 2017, American Chemical Society.

dissolve in organic polymeric matrices and easy to aggregate. Ji, Wei, and co-workers introduced well-dispersed organic polydopamine nanoparticles as the photothermal agent into the LCE polymer matrix without any additional additive or treatment, which was attributed to the numerous amino and hydroxyl groups on surface (**Figure 9**a).[39] In addition, polydopamine nanoparticles also displayed excellent photostability, strong absorption of NIR light, and negligible resonance light scattering in the NIR region, contributing to the high efficiency of photothermal conversion. The temperature of the LCE sample reached 160 °C in 15 s upon irradiation with an 808 nm wavelength laser (1.4 W cm^{-2}), which enabled the planar aligned LCE to perform a reversible actuation as the light was switched on and off (Figure 9b). Moreover, based on the transesterification between hydroxyl groups and eaters triggered by light, the LCE sample can be reshaped and healed.

The poor solubility of the photothermal agents is the main disadvantage of the physical blending strategy in organic polymeric matrices. It is noted that low doping percentages will decrease the response speeds of the LCP actuators, whereas high doping percentages will lead to the inhomogeneous dispersions and phase segregations. Yang and co-workers reported a main-chain LCE chemically bonded with NIR absorbing chromophore crosslinkers, which exhibited an ultrafast photoresponsive speed and superior mechanical property.[40] The LCE material surface temperature rapidly increased over the LC-isotropic transition (116 °C) in 2 s and raised its local temperature from 18 to 260 °C in less than 8 s upon exposure to 808 nm NIR stimulus (0.83 W cm^{-2}). Based on the extraordinary photothermal conversion property, an LCE ribbon hung up with a binder clip shrunk upon NIR light irradiation and expanded to the original state when the NIR stimulus was switched off. Taking advantage of the main-chain end-on mesogenic structure, the LCE ribbon achieved a large and reversible shrinkage of about 110% at the LC-isotropic phase transition (Figure 9c). The Young's modulus of the LCE film in the isotropic phase could still maintain at ≈1.4 MPa, which increased by nearly one order of magnitude compared with that of traditional side-chain LCE soft actuators (30–300 kPa). Based on the robust mechanical property, this novel LCE material had an outstanding ability to lift heavy objects. Upon exposure to NIR light, the LCE film (4.3 mg) lifted up heavy loads of one counterpoise and two binder clips (≈24.440 g), which was 5680 times heavier than itself.

The frequently used photothermal agents and their maximum temperature under light irradiation are briefly summarized in **Table 1**. When azobenzene derivatives are used as photoresponsive moieties in the LCPs, the photomechanical and photothermal contributions to actuation in different situations has been investigated.[41] Through a combined mechanical and kinetic analysis of splay-aligned LCN films with three commonly used azobenzene chromophores in air and water, Schenning and co-workers uncovered that the governing factors in the photodeformation mechanism depend on the chemistry of the chromophore, including location (side-chain or crosslinker), lifetime of *cis* isomer, and structures of polymer networks.[42]

3. Complex Deformation

The driving force for most large changes of LCPs in shape arises from a variation of LC alignment order.[43] The principle underlying the deformations is conceptually simple: if there is no director reorientation and no generation of free volume, an aligned system must always contract along the director and expand perpendicular to it when brought into a state of lower order.[44] Bending is the simplest deformation in the LCPs, which is induced by an asymmetric contraction or expansion. The initial alignment of the mesogens strongly affects the bending behavior. Ikeda and co-workers incorporated azobenzene

Table 1. Summary of the frequently used photothermal agents in LCP systems.

Materials	Content	Maximum temperature under light irradiation	Light intensity	Ref.
1-AM[a]/LCN	1.5 wt%	45 °C	405 nm (152 mW cm^{-2})	[35]
YHD796C[b]-LCE	17.0 wt%	260 °C in 8 s	808 nm (0.83 W cm^{-2})	[40]
Disperse Orange 3/LCE	1 wt%	–	532 nm (5.5 W)	[66]
Azo-LCN	20 wt%	100 °C	320–500 nm (200 mW mm^{-2})	[70]
Gold nanorod/LCE	1.0 wt%	44.2 °C in 5 s	635 nm (95 W cm^{-2})	[38]
PDA[c]/xLCE[d]	2.0 wt%	160 °C in 15 s	808 nm (1.4 W cm^{-2})	[39]
PDA coated LCN	–	171 °C	808 nm (4 W cm^{-2})	[79]
Azo dye-LCE	1 mol%	100 °C	532 nm (10 W mm^{-2})	[68]
Disperse Red 1/LCN	1 mol%	–	470 nm (320 mW cm^{-2})	[71]
Disperse Red 1-LCN	7 mol%	100 °C	405 nm (510 mW cm^{-2})	[81]
Disperse Red 1/LCE	2 mol%	47 °C	488 nm (130 mW cm^{-2})	[67]
	4 mol%	49 °C in 30 s	470 nm (230 mW cm^{-2})	[85]
SWNT[e]/LCE	0.1 wt%	8 °C in 10 s	980 nm (11.0 mW mm^{-2})	[65]
	0.45 wt%	–	white light (230 mW cm^{-2})	[84]

[a]1-AM: Azomerocyanine dye; [b]YHD796C: NIR absorbing crosslinker, 2,5-bis[(1-dec-9-enyl-undec-10-neyl-4-carboxylate-piperidyl-amino)-thiophenyl] croconium; [c]PDA: polydopamine; [d]xLCEs: liquid crystalline elastomers with exchangeable links; [e]SWNT: single-walled carbon nanotubes.

chromophores into LCEs and demonstrated different bending direction of the films with homogeneous and homeotropic alignment upon light irradiation.[45] When exposed to UV light at 366 nm (50 mW cm^{-2}), the homogeneous film bent toward the irradiation direction of the actinic light along the alignment direction, while the homeotropic film bent away from the light source. In the homogeneous films, an anisotropic contraction of the surface layer was generated along the direction parallel to the alignment of the azobenzene mesogens. On the other hand, the azobenzene mesogens were perpendicular to the film surface in the homeotropic films; thus, exposure to UV light induced an isotropic expansion of the surface layer.

Given an order-reducing stimulus, uniaxially oriented systems only contract by a small amount parallel to the director. Twisted systems, however, bend out of the plane of the film with a much larger amplitude.[46] One alignment configuration, the 90° twist, which maximizes bending deformations, is that the director is oriented parallel to the film in one surface while the director is perpendicular to the film in the other surface. Harris et al. fabricated the actuators containing azobenzene moieties with a densely crosslinked, twisted configuration.[47] During the UV irradiation, the films contracted along the director and expanded in the perpendicular directions, as is consistent with a UV-induced decrease in order when the azobenzene undergoes *trans–cis* photoisomerization. The expansion/contraction anisotropy creates a helical character in the films, which becomes especially pronounced when the length to width radio of the active films becomes larger.

Moreover, by introducing chiral dopants into the LC mixtures to prevent the formation of multiple alignment domains, a consistent right- or left-handed twist sample can be produced. Katsonis, Fletcher, and co-workers also designed the photoresponsive LCP springs based on azobenzene, in which molecular movement is converted and further amplified into controllable twisting actuations.[48] A small amount of the chiral dopants was added into the LC mixtures to favor a left-handed or right-handed twist. The orientation of the LC director in the films varied smoothly by 90° from one surface to another (**Figure 10**a). The films spontaneously coiled into various helical shapes with diverse pitches when they were cut into ribbons because of the competition among three sources of asymmetry, including handedness of the director twist, the cutting direction, and gradient in density. Under irradiation with 365 nm UV light (60 mW cm^{-2}), the ribbons contract along the director and expand in the perpendicular directions, displaying winding, unwinding and helix inversion (Figure 10b). The deformations were reversible at room temperature with relaxation times of a dozen minutes, which could be accelerated to completion in a few seconds by visible light (≥420 nm). Moreover, a continuous push–pull motion was demonstrated by using a tendril-like ribbon clamped at each end upon alternate exposure to UV and visible light. Furthermore, they used crosslinkers containing *ortho*-fluorinated azobenzene as photoswitchable moieties instead of the normal azobenzene to fabricate LCNs, which constituted the demonstration of long-lived photomechanical deformation that retained for more than eight days.[49]

Nature uses molecular-scale machines to drive every significant biological process and powers macroscopic mechanical motion in plants in highly complex process, which often relies on dynamic helical systems. Plant pods typically possess a flat hull composed of two narrow sides with two fibrous layers aligned at opposite angle, when the pod dries, each fibrous layer shrinks and curls into helical strips of opposite handedness and eventually a dramatic opening.[50] In analogy, Katsonis, Fletcher, and co-workers prepared the helical strips based on LCNs patterned with periodically alternating bars to mimic the opening of pod.[51] One set of bars was polymerized in a low LC order state, because *trans–cis* photoisomerization was also triggered in process of photopolymerization, whereas

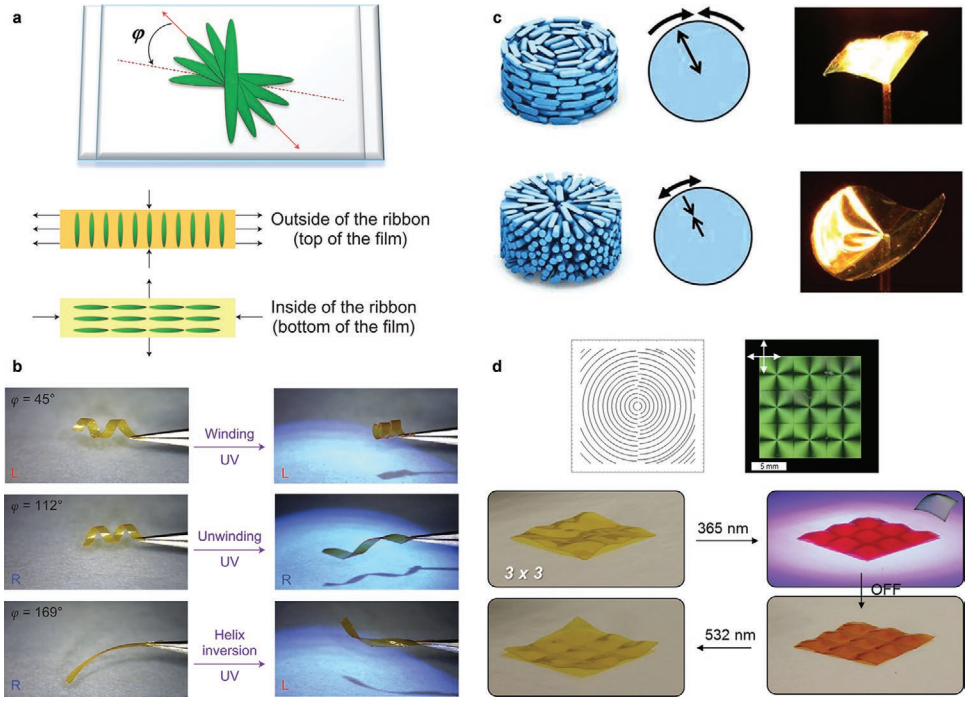

Figure 10. a) Molecular organization in the twist cell and the angular offset φ, which characterizes the angle at which the ribbon is cut. The orientation of the molecules at mid-plane is shown with a double-headed arrow. The cutting direction, which is also the long axis of the ribbon, is represented by a dotted line. The elongated rods represent molecules. The ribbons deform to accommodate the preferred distortion along the main axis of the ribbon, and this preferred distortion is determined by the orientation of the molecules. b) Spiral ribbons irradiated for 2 min with ultraviolet light ($\lambda = 365$ nm) display isochoric winding, unwinding and helix inversion as dictated by their initial shape and geometry. Reproduced with permission.[48] Copyright 2014, Springer Nature. c) Actuation behavior of an azimuthal polymer film (top) and a radial polymer film (bottom) upon heating with an IR lamp. The arrows along the radius and the azimuth indicate the direction of deformation. Reproduced with permission.[52] Copyright 2012, Wiley-VCH. d) A 3 × 3 array of +1 azimuthal defects is prepared in an azo-LCE. Upon irradiation with 365 nm light, nine conical domes emerge from the film. The cones are metastable after removal of the UV light before being returned to the flat state by irradiation with 532 nm light. Reproduced with permission.[54] Copyright 2016, Wiley-VCH.

the other bars were polymerized without isomerization to retain a high LC order. Various shapes of the bar-patterned film were obtained depending on the cutting angle, including flat strips and helicoids. Initiated by photochemical isomerization under 365 nm light illumination (290 mW cm^{-2}), the two sets of bars underwent different shape and size modifications. In highly ordered bars, *trans–cis* isomerization induced expansion preferentially perpendicular to the director, and this specifically translated into an elongation of the bars. The elongation of disordered bars was consequently negligible under stimulation. These shape transformations induced the twisting of LCN strips to compensate for strain. By assembling two mirror-image strips cut from one LCN film (such as the strips cut at 45° and 135°), an artificial pod was fabricated, where each strip acted as the valve. Under illumination, the valves bent along the short axes to generate a hollow cavity in their center, where strain built up slowly and accumulated until the valves suddenly detached from each other, twisted into springs, and the pod opened. The total operation process took about 40 s.

Molecular director of the abovementioned LCPs only varies in one direction, i.e., twisted alignment, which causes curl under light stimulus. More complex patterning of the LC alignment could be realized by using photoalignment method to prepare special alignment layers with the aid of photomasks. Broer, Schenning, and co-workers demonstrated the well-defined deformation in three dimensions of LCNs with patterned alignment via the photothermal effect.[52] By slowly rotating the cell while exposed to linear polarized light through a photomask with a wedge-shaped opening, a series of different cells with a continuous change of the alignment direction were prepared, such as an azimuthal alignment and a radial alignment.[53] The film with azimuthal alignment deformed into a conical shape with the cone apex located at the center. A photothermal-induced reduction of the LC order led to the contraction along the azimuthal direction and the expansion along the radial direction respectively. These stresses were not able to be accommodated within the sheet plane, which gave rise to deformation of the flat sheet into a cone. On the contrary, the opposite deformation takes place in the radial alignment film, which deformed into a saddle shape (Figure 10c). Besides, White and co-workers also demonstrated reversible shape change in azo-LCE films with defect arrays based on photochemical phase transition.[54] The film with a 3 × 3 arrays of +1 azimuthal defect deflected and formed the conical deformation upon irradiation with 365 nm light (Figure 10d). It was found that although the birefringence of topological +1 and −1 taken between cross polarizers were indistinguishable (four brushes), their resulting shape change were markedly different dictated by the distinct differences in the director profiles. Moreover, the deformation

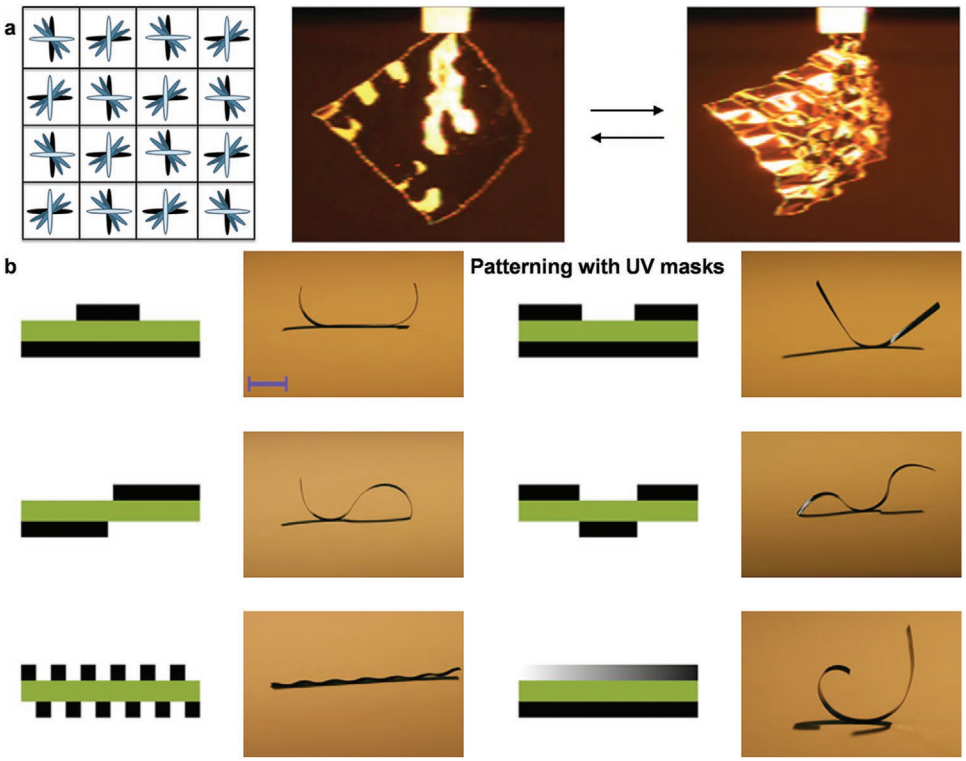

Figure 11. a) Top view of the final pattern of the checkerboard alignment layers (only 4 × 4 squares shown) and deformation upon IR heating of a film with a checkerboard pattern. Reproduced with permission.[55] Copyright 2014, Wiley-VCH. b) Schematic of mask patterns (left) and photothermally induced shape morphing upon red light illumination after different mask exposure. Scale bar, 5 mm. Reproduced with permission.[56] Copyright 2018, Springer Nature.

of azo-LCEs strongly depends on the azobenzene concentration as well as the crosslink density.

Furthermore, Schenning, Broer, Selinger, and co-workers prepared patterned LCN actuators with a 3D director variation, which feature a discrete alternating striped or checkerboard director profile in the plane and a 90° twist through the depth.[55] In discrete alternating striped films, the alignment of the mesogens in adjacent strips were opposite. For example, the mesogens in stripes 1 and 3 were oriented along the long axis of the film at the top surface, but were oriented along the short axis at the bottom surface. Stripes 2 and 4 had the opposite director profile, which was along the short axis at the top and along the long axis at the bottom. Upon irradiation with an IR, the LCN in each stripe expanded on one side and contracted on the other side along the long axis. Consequently, the stripes bent in opposite directions upon actuation to generate accordion-style folds. To extend more complex deformation, the film was prepared with two orthogonally superimposed lane masks to make a checkerboard pattern. Upon IR irradiation, the film with the checkerboard pattern deformed from a mostly flat shape to form a periodic square pattern of peaks, depressions and saddle points (**Figure 11**a). Such 3D deformation of the actuators could offer new ways to perform auto-origami and achieve a total displacement larger than that could be accomplished by the contraction of a planar aligned sample with uniform nematic director.

Hitherto, the LCNs with unidirectional, twisted, and circular director profiles will contract, bend, or curl, and deform into cone or anticone shapes respectively when a light stimulus is applied. Other interesting reversible deformation has been also achieved by imposing a 3D director profile on the film, with variation through the thickness as well as in the plane of the polymer film. Priimagi, Zeng, and co-workers demonstrated a planar-aligned LCN strip with six different reconfigurable deformations through synergistic use of photochemical and photothermal responses within a single LCN actuator.[56] The photoisomerization of azobenzene moieties was used to locally control the *cis*-isomer content and to program mechanical properties of the actuator (no shape changes), whereas the photothermal effect triggered shape changes upon red light irradiation by releasing the stress originating from inhomogeneous distribution of the *cis*-azobenzene. Firstly, spatially pattering via masked 365 nm UV illumination from either one side or both sides of the LCN film allowed for local control over the *cis*-isomer content, thus programming the actuator performance. In this process, the preirradiation of the UV light led to negligible shape change of the film, and the photochemically induced stress was "hidden" inside the LCN actuator. Subsequently, photothermal heating stimulated the UV-encoded actuation capacity, giving rise to diverse deformation upon 660 nm red light irradiation (Figure 11b). All the shapes are generated within the same film after recovery to the initial flat state by irradiation with 460 nm blue light to convert the *cis*-form back to the *trans*-form.

Functional coatings with switchable surface topographies are in great demand for a wide variety of applications, for which wettability, optical properties (scattering, diffraction, and reflection), and mechanical properties (friction, stick, and adhesion) are all

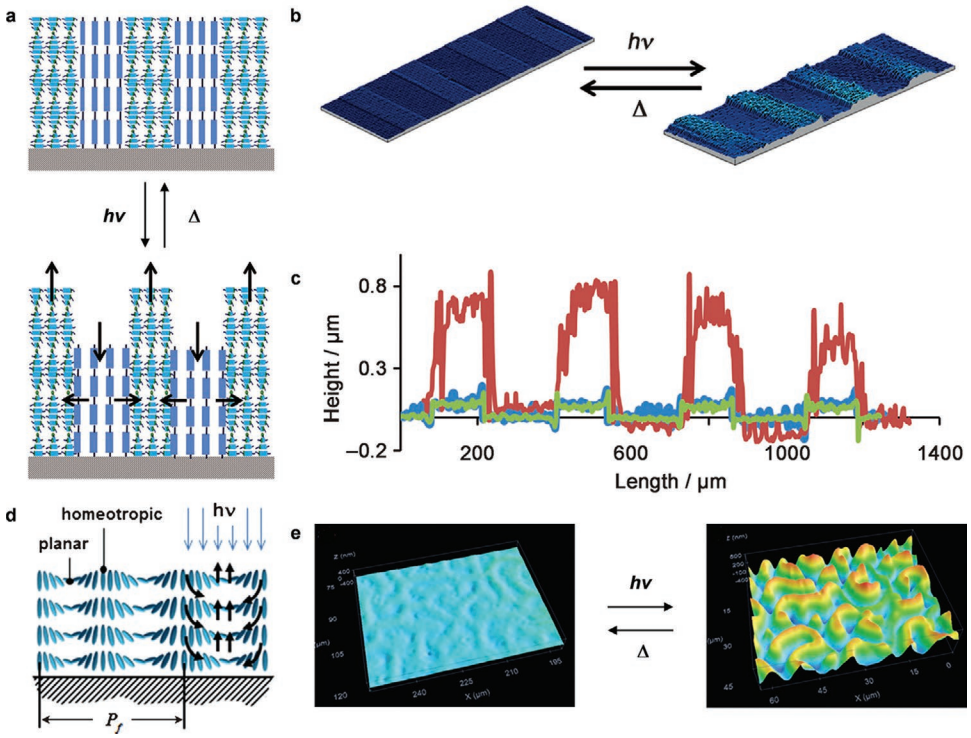

Figure 12. a) LCN containing striped patterns of alternating areas with chiral nematic order and homeotropic orientation. Upon exposure the chiral nematic areas expand perpendicular to the plane of the film and the homeotropic areas contract in the perpendicular direction. In the plane of the film the chiral nematic areas contract and the homeotropic areas expand. b) 3D images of surface topologies at the original state (left) and during illumination with UV light (right). c) Surface profiles of the initial profile (blue), during UV illumination (red), and after removal of the illumination (green). Reproduced with permission.[58] Copyright 2012, Wiley-VCH. d) Schematic representation of the dynamics of the fingerprints. e) Confocal microscopic images of the initial flat state and surface topographies under UV exposure. Reproduced with permission.[59] Copyright 2014, Wiley-VCH.

related to the surface structures. Azobenzene-copolymerized LCNs have been mainly studied for the photoresponsive coatings, which demonstrate reversible change of surface topographies between flat and corrugated states in micrometer range when confined on a rigid substrate.[57] The mechanism of the anisotropic dimensional surface deformation is based on the order parameter reduction and free-volume effect by a photoinduced isomerization of the azobenzene in LCNs. Broer, Liu, and co-workers reported photoswitchable surface topologies by integrating azobenzene-containing crosslinkers into a structured chiral nematic network.[58] To enhance the depth of the surface modulation, areas with homeotropic molecular alignment were alternatively integrated into the chiral nematic LCN film (**Figure 12**a). The coexistence of the chiral nematic and homeotropic phase could simply be realized by the use of patterned indium tin oxide electrodes. The two types of molecular order had opposite photo–mechanical responses, which was induced by cooperative disordering of the aligned molecules with conformational change of azobenzene units. The chiral nematic areas, where the molecules were oriented on average planar to the surface, expanded perpendicular to the film surface under irradiation of 365 nm UV light (30 mW cm^{-2}), whereas the homeotropic areas contracted (Figure 12b). When the UV light was switched off, the initial flat surface was retained within seconds. The degree of strain perpendicular to the surface demonstrated a large deformation reaching close to 20% (Figure 12c). Furthermore, they demonstrated reversibly switchable 3D fingerprint surface topographies in azobenzene-based chiral nematic LCN coatings, where the molecular helixes were parallel to the substrate (Figure 12d).[59] When addressed with 365 nm UV light (400 mW cm^{-2}), the surface formed protrusions at the planar positions and withdraws at the homeotropic positions (Figure 12e), resulting in a large height difference up to 24%. The relaxation to the initial flat state occurred within 60 s. By tuning the friction force of the LCN coatings based on the switchable artificial fingerprints, robotic fingers were built to grip and release objects.

Instead of using complicated method to produce localized alignment or carefully balancing the chiral force and the anchoring force in chiral nematic LCN coatings, Broer and coworkers described an easier self-assembling way to fabricate the surface-responsive coatings based on randomly ordered polydomain azo-LCN.[60] The domains with varying directors were generated by the introduction of a nonsoluble monomer, which disturbed the molecular order of the LC. When attached to a solid substrate, the coating underwent a change from a flat state to a jagged state upon irradiation of UV light, showing a significant depth modulation of more than 20%. The smaller domain size, the rougher and spikier coating surface.

The initial LC alignment plays a key role in enabling the distinctive ability to generate complex shape changes, which is controlled by external boundary situations (surface-alignment layers, surfactants) and stimuli (magnetic, electric, and optical fields).[3a,61] The capability to control the 3D structures of the LC

mesogens in polymers has created numerous intriguing actuators for potential applications in self-cleaning surface, autonomously adjusting lenses, haptic robots, and microfluidic systems.

4. Light-Fueled Actuators

The ability to create the mechanical work remotely, with high speed and spatial precision, provides numerous intriguing possibilities. Recent developments in photoresponsive LCPs are at the heart of these future devices.[62] In this section, the soft actuators of the LCPs are classified according to the actuation mode and their applications.

4.1. Locomotion

Soft animals such as snails, earthworms, and larval insects are capable of deforming their bodies to navigate in complex 3D topographies and to accommodate to the environmental confinements. This approach to locomotion has inspired scientists and engineers to seek similar strategies for walking soft robots. Light-fueled soft robots require a strategy to transfer photomechanical deformation into locomotion, which is different from microdevices driven by external forces or torques, hence the locomotion is totally determined by the interaction between the robot body and its environment. Photoresponsive LCPs with programmed anisotropy could mimic the anisotropic mechanics in numerous natural examples of locomotion.[63] Various LCP actuators exhibiting caterpillar-like motion such as rolling, inching, and travelling-wave movement are achieved.

Ikeda and co-workers prepared bilayer films consisting of a homogeneously planar aligned azobenzene-containing CLCP and a plastic sheet to achieve an inchworm walk.[64] The bilayer film was initially curled because of the difference in the thermal expansion coefficients between the two layers. By designing asymmetric end shapes, a sharp edge and a flat edge, the film moved forward to the flat edge upon alternative exposure to UV and visible light at room temperature. Upon exposure to 366 nm UV light (240 mW cm^{-2}), the film extended forward because the sharp edge acted as a stationary point, and the film contracted from the rear side upon exposure to >540 nm visible light (120 mW cm^{-2}) since the flat edge served as the stationary point, which allowed the film to move in only one direction.

Based on the similar design, Kohlmeyer and Chen demonstrated an IR light-fueled inchworm walker, which could crawl up a hill at a 50° incline.[65] The inchworm walker was composed of an asymmetric SWNT-LCE/silicone bilayer film and two polycarbonate films with different shapes (**Figure 13**a). Upon 980 nm NIR irradiation, the tightly bound SWNT-LCE layer underwent a significant in-plane negative strain, which bent the underlying silicone elastomer layer, i.e., the film bent to the SWNT-LCE layer. The IR-induced bending mainly originates from the N–I phase transition (64.6 °C), which reached over 80 °C soon after the IR light is turned on. On the tilting ratcheted substrate (50°), the sharp side of the bilayer film as the stationary point bent outward, when irradiated by NIR light (28.2 mW mm^{-2}) at the first half of the film. Then, the NIR light was moved to the center of the bilayer film, causing the flat side bent inward, so that the second half of the film slid forward. Finally, the NIR light was turned off, which allows the whole bilayer film to unbend and the first half of the film to slide forward.

Instead of constructing the bilayer walkers with additional asymmetric surface to create movement tendency, Wasylczyk and co-workers fabricated a caterpillar robot based on a single photoresponsive LCE monolith by mimicking the caterpillar terrestrial locomotion with wave mode.[66] The caterpillar robot was made of an elastomer strip with alternately patterned molecular alignment, where the areas molecules aligned preferentially faced the areas molecules oriented randomly. Under irradiation with 532 nm light (5.5 W), rearrangement of the molecules induced by photothermal phase transition resulted in expansion of the areas in the well-oriented segments, leading to that the flat film became curly. To achieve the travelling deformation, a laser beam was first projected on the tail and the caterpillar robot deformed into a curved shape, lifting from the ground and shortening at the same time. By scanning the laser beam toward the robot's head, the deformation followed. After the laser beam completed the scan, the robot returned to the original flat state, thus completing one step forward in the stepping cycle with an average speed of 0.24 mm s^{-1} (Figure 13b). Moreover, the robot can execute various tasks such as walking up a slope, squeezing through a narrow slit, and pushing objects. Besides, Priimagi, Zeng, and co-workers also reported a caterpillar robot made of monolithic LCE elastomer film, which was composed of three alternating splayed-aligned segments that gives rise to a "Ω"-like geometry.[67] Upon 488 nm light illumination (150 mW cm^{-2}), the light energy absorbed by photothermal agent Disperse Red 1 was transferred into heat inside the LCE, making the curved structure become flat and resulting in extension of the body. When the light was switched off, heat released to the environment, and the robot recovered to its original shape. Therefore, cycling of actuator between the curled and flat stages resulted in photoinduced locomotion.

A miniature-sized robot has a small mass, resulting in limited inertia, hence the motion is dominated by forces related to the surfaces, such as adhesion, friction, or drag. Most of the crawling LCE soft robots reported are in the centimeter or millimeter scale, because when the entire size shrinks down to micrometers, the adhesion becomes compared with the elastomeric force of LCE, posing a great difficulty for any movement. By mimicking muscles, whose hard crust and hairy-like surfaces often assist to reduce the surface contact zone and hence minimize the biological adhesion, Wiersmag, Zeng, and co-workers used direct laser writing system to fabricate a microscopic walker with four limbs composed of acrylic resin to solve the adhesion problem (Figure 13c).[68] Shape of the limbs was chosen as conical to reduce the surface contact area, whereas 45° tilt created the adhesion asymmetry necessary for walking. Under the modulated 532 nm laser beam (50 Hz, 10 W mm^{-2}), photothermal phase transition was induced in the planar-aligned azo-LCE body, resulting in the contract-expand reversible deformation. The microscopic walker could automatically perform various locomotion highly depended on the friction differences from one leg to the other (Figure 13d). Therefore, the microscopic walker showed a random walking behavior on the nonuniform polyimide coating with different

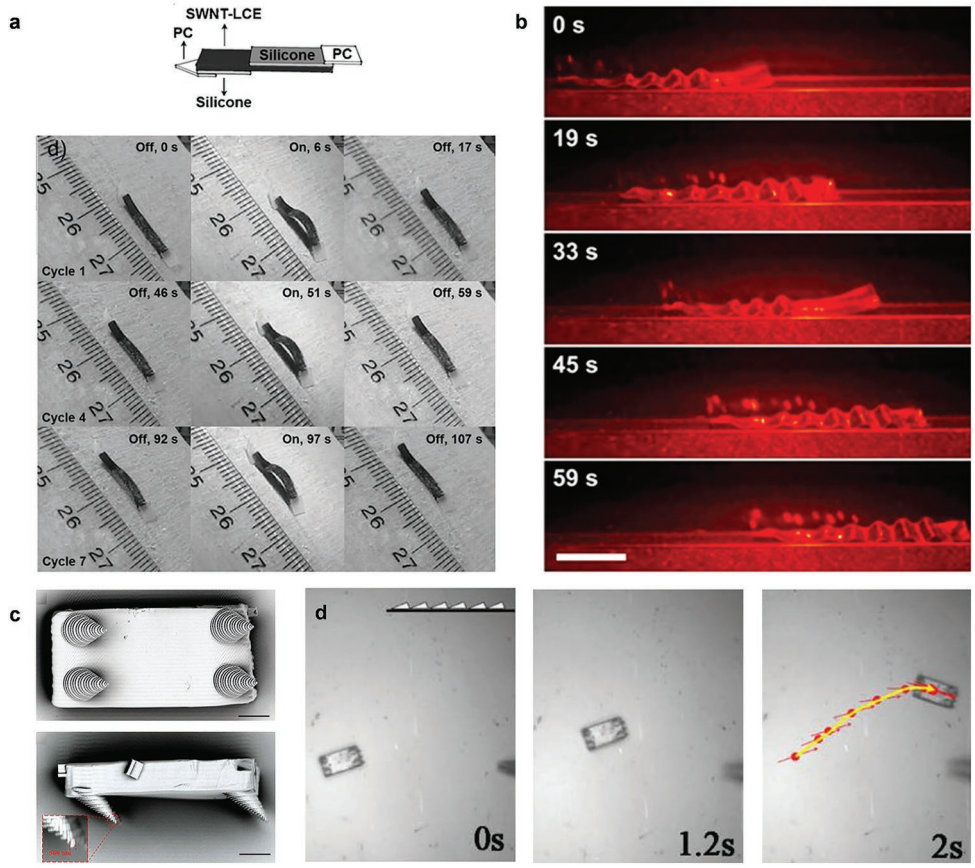

Figure 13. Light-fueled locomotion. a) Scheme of an inchworm walker device consisting of an asymmetric SWNT-LCE/silicone bilayer film. The inchworm walker crawls up the wood substrate at a 50° incline in response to on and off cycles of continuous-wave NIR light (28.2 mW mm^{-2}). Reproduced with permission.[65] Copyright 2013, Wiley-VCH. b) Series of photographs for the photoinduced locomotion in the forward directions. Scale bar, 5 mm. Orange filter is used to cut off scattered green light. Reproduced with permission.[66] Copyright 2016, Wiley-VCH. c) SEM image of a microwalker lying upside down (top) and side view of the microwalker with 500 nm leg tip shown in the inset (bottom). Scale bar, 10 µm. d) Surface dependent locomotion behaviors. Under the chopped laser excitation (532 nm, 50 Hz, 10 W mm^{-2}), the 60 µm size microwalker walks in the direction determined by the grating groove pattern (vertical). Reproduced with permission.[68] Copyright 2015, Wiley-VCH.

local fluctuations of the adhesion, whereas on a clean glass substrate the actuator moved with a preferred direction defined by the leg tilt due to the shear off anisotropy.

Different form crawling, rolling LCP soft robots always move based on asymmetric deformation, which induces a shift of the center of mass and produces a torque that drives the LCP robots rolling. Ikeda and co-workers first reported photoinduced rolling motion of a continuous ring of the LCE film prepared by connecting both ends of the film.[69] The azobenzene mesogens were aligned along the circular direction of the ring. Upon irradiation with UV light from the downside right and visible light from the upside right simultaneously, the ring rolled intermittently, resulting almost in a 360° roll at room temperature. Similarly, White and co-workers reported photoinduced rolling motion of strips, which is prepared from azobenzene-functionalized LCNs.[70] The azo-LCN strips prepared in twisted nematic conformation were first generated a spiral shape under irradiation of 320–500 nm light (200 mW cm^{-2}), and then sustained motion under continued irradiation, which originated from the photochemical conformational change with contribution from absorptive heating. When irradiated from above, upper portion of the azo-LCN film lost nematic order induced by the *trans–cis* isomerization and adopted a greater twist in comparison to the portion where light was shadowed, which broke symmetry of the spiral. The direction of the motion is affected by the helical angle, which is manipulated by the alignment of the nematic director to the surfaces of the azo-LCN.

Multigait rolling movement of a 3D kirigami-based rolling LCN robot with multiple petals containing photothermal dyes was demonstrated by Zeng and co-workers, including navigation along different routes and climb on a slope with an inclination up to 6°.[71] Series of stripes were laser cut along the planar direction of the splay-aligned film, forming the petals for the locomotion. The cut film was then rolled up into a tube and reinforced by a plastic ring. Upon symmetrical 470 nm light irradiation through the glass substrate (320 mW cm^{-2}), the petals on both sides bent toward to the light and pushed the ground, inducing sequential forward-rolling motion. Interestingly, when the light spot was concentrated to one side of the petals, the robot turned the rolling direction and could be manually steered to navigate along designed pathways. The kirigami technique suggests a facile technique to fabricate complex

geometries in designing light-fueled rolling devices and other soft microrobotics.

Unlike the actuators with single locomotion mode mentioned above, Zeng, Cheng, and co-workers elicited diverse underwater locomotion, including crawling, walking, jumping, and swimming, into photothermal-driven LC gels by mimicking the phylum Mollusca.[72] The splay-aligned LC gels were prepared by adding certain amounts of 5CB into the LCN precursor. Activated by the photothermal effect, the molecular alignment in LC gels decrease, inducing temporal macroscopic shape morphing and the storage of elastic energy. The release of elastic energy during relaxation results in the displacement of the surrounding fluid and the subsequent underwater locomotion. Importantly, with the gradual addition of 5CB, both stiffness and density of the LCN reduce, promising a larger magnitude of thermal actuation and buoyancy in water. By combining external solids as support, the LC gels with 50 wt% 5CB can generate undulatory traveling waves for crawling upon irradiation of 532 nm light (below 1.8 W cm^{-2}) at a certain angle. The LC gels can also walk on a ratchet surface upon irradiation at a point away from the geometrical center, where the leg closer to the illuminate spot deforms to a larger extent than the other, inducing an asymmetry in bending and friction for the forward locomotion. As the weight percentage of 5CB increases to 70 wt%, the LC gels show sharper phase transition and lower density, so that the stored elastic energy upon illumination is larger enough to lift the gels and result in jumping behavior and even swimming by slightly salting the water.

4.2. Oscillation

The oscillation is based on a laser beam hitting the two surfaces of the actuator strip alternately, inducing bending actuation that deflects the strip inside and outside of the confined irradiation area. The key to self-oscillation is the time delay in the material response: while an oscillator passes through the equilibrium, the delayed force remains in the system showing the same direction as the velocity, thus pushing the object out of the equilibrium and providing positive feedback to the motion. The feedback extracts the energy form the external energy source (light), fueling the oscillator to sustain the motion.[73] Bunning and co-workers reported the fast and large-amplitude (>170°) oscillation of a light-fueled cantilever consisting of a planar-aligned monodomain azo-LCN.[74] A polarized laser beam (0.8 W cm^{-2}) was used to drive both *trans–cis* and *cis–trans* isomerization, resulting in realignment of molecules perpendicular to the polarization direction according to Weigert effect (Figure 6a), and thus contraction of the azo-LCN along the direction of the polarization. Upon exposure to the polarized laser beam, the LCN film first bent toward the light. When the moment of the inertia of the LCN cantilever above a threshold that enables the cantilever to deflect the path of the light, the back surface of the LCN was exposed to light. Then contraction occurred on the back surface of the LCN reversed the displacement direction, resulting in oscillatory motion (**Figure 14**a). The frequency of the oscillation was nearly 30 Hz (Figure 14b), which was similar to that of a hummingbird wingbeat ranging from 20–80 Hz, and the behavior showed little fatigue over 250 000 cycles. After optimization of the strip size, thickness, and excitation power, an oscillation frequency as high as 270 Hz was reached.[75]

Furthermore, White and co-workers added dimensionality to the in-plane bending oscillations to create flexural–torsional oscillations in cantilevers also based on Weigert effect.[76] The flexural–torsional oscillations were composed of 3D movement encompassing both in-plane bending and out-of-plane twisting. The cantilevers were fabricated based on monodomain glassy azo-LCN, where the alignment of the nematic director in the cantilever could strongly influence the dimensionality of the oscillations. When the nematic director was parallel to long axis of the cantilever, the material exhibited in-plane bending oscillation, whereas the material exhibited asymmetric bending but not oscillation when the nematic director was perpendicular to the cantilever axis. As the alignment of nematic director was rotated with respect to the long axis of the cantilever, flexural–torsional oscillations occurred. The out-of-plane twisting resulted from a photogenerated shear gradient through the thickness of the LCN cantilever. The exposed surface contracted to a greater extent along one diagonal of the cantilever than the other, leading to shear. Under exposure to polarized light from a 442 nm coherent wave laser (1.1 W cm^{-2}), the frequency of the cantilever reached up to 120 Hz. Moreover, the amplitude of the oscillation increased from 20° to 90° as laser intensity increase from 1 to 1.5 W cm^{-2}.

A sunlight-fueled oscillating soft actuator on the basis of splay-oriented LCN film using photopolymerizable *ortho*-fluoroazobenzene was developed by Schenning, Debije, Bléger, and co-workers.[77] The chaotic self-oscillation was caused by a coupling of the periodic small variation of the *cis*/*trans* population and their isomerization rates, as a proper mix of simultaneous green (157 mW cm^{-2}) and blue (318.8 mW cm^{-2}) light irradiation was necessary to generate the oscillatory behavior. When suspended the film under sunlight (35 mW cm^{-2}), the LCN film displayed a continuous and fully reversible actuation with bending angles ranging from –2° to 12° (Figure 14c).

By taking advantages of the photothermal effect, Broer, Meijer, and co-workers demonstrated a steady self-oscillation of splay-aligned LCN cantilevers.[78] When the 365 nm LED light (≥450 mW cm^{-2}) hit the localized zone (hinge), the LCN film bent at the hinge as the temperature increased. After the tip of the bending film shadowed its hinge, the hinge cooled down and the film reversed to its resting position and placed the hinge in the light beam again. Thus, self-oscillation of the LCN film was realized (Figure 14d). The frequency of the oscillation was 6.3 ± 0.3 Hz, and the amplitude defined as the displacement in the *z*-direction of the tip reached 8 mm (Figure 14e). One should be emphasized that the use of a collimated light beam was crucial to enter in the self-sustained oscillation regime, whereas a diffuse source led to bending of the whole film. By incorporating other photothermal agents of different maximum absorption wavelength into the LCN, steady self-oscillations can be triggered by light from 365 to 600 nm.

Based on the same self-oscillation movement mechanism, Yang and co-workers designed an 808 nm NIR-light-fueled oscillator by selectively coating a polydopamine polymer layer on the surface of a splay-aligned LCN film, where the position coated by polydopamine acted as the hinge.[79] The frequency

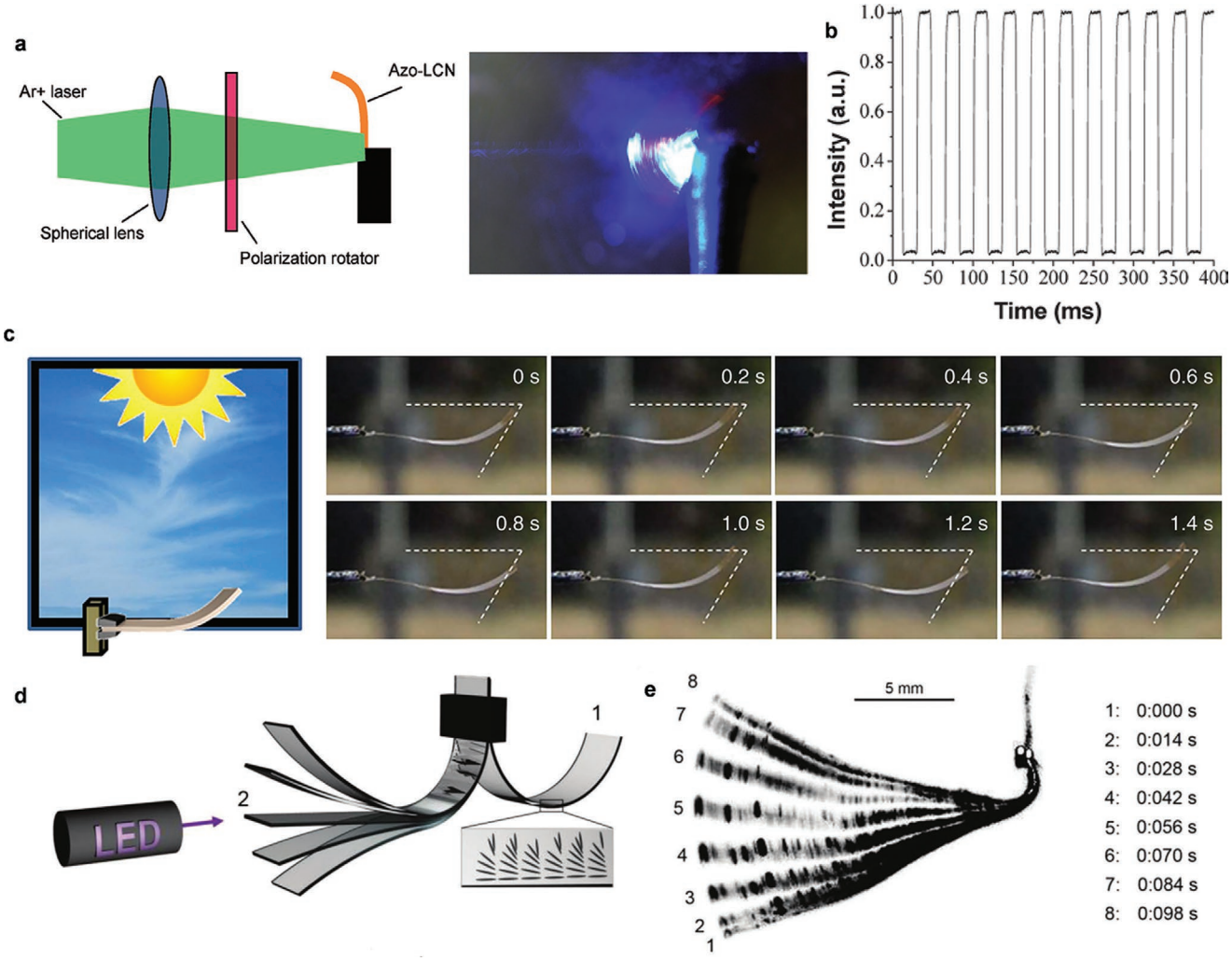

Figure 14. Self-oscillation. a) Schematic illustration showing the simple optical setup for photoinduced oscillation (left) and the oscillation driven by a 442 nm laser beam (right). b) The frequency of the oscillating cantilever measured optically and determined to be 28.4 Hz. Reproduced with permission.[74] Copyright 2008, The Royal Society of Chemistry. c) Experimental setup for measurement of oscillatory motion of a photomechanical film during sun exposure (left) and series of snapshots extracted from the video depicting film oscillations; dotted lines have been added to aid the eye (right). Reproduced with permission.[77] Copyright 2016, Springer Nature. d) Schematic representation of the setup and the splay alignment (inset). Initially the film is curved (position 1). When the light is switched on, the film bends toward the light (position 2) where it starts oscillating. e) Overlay of frames showing oscillation of the film, irradiated from the left with UV light (LED 365 nm, 0.52 W cm^{-2}). Reproduced with permission.[78] Copyright 2017, Wiley-VCH.

of the oscillation reached 9 ± 0.4 Hz under irradiation with intensity of 2.5 W cm^{-2}, and the reversible motion with tip displacement ranging from 0 to 8.4 mm when the intensity of the light was 2.1 W cm^{-2}. Especially, polydopamine used as effective photothermal materials presents superior adhesion and is able to be feasibly removed by alkaline solution, which makes the oscillation of the LCN film reprogrammable by repeatedly coating and washing.

4.3. Self-Sustainable Motion

Mimicking the autonomous and continuous (i.e., self-sustainable) motion of smart biological systems in nature has attracted much attention but proved challenging. Light-fueled self-sustainable motion is defined as that actuators can execute continuous actions without constantly controlling the light source in a spatial and temporal sense. Photoresponsive LCPs offer great potential to integrate individual functional parts into a single sheet.

Ikeda and co-workers first reported the continuous rotational motion of a photoinduced plastic motor by using a laminated film consisting of an azobenzene-containing LCE and a flexible polyethylene (PE) sheet.[69] The plastic belt was fabricated by connecting both ends of the film, and then placed on a homemade pulley system (**Figure 15**a). By irradiating the belt with UV light from top right and visible light from top left simultaneously, a rotation of the plastic belt was triggered to continuously drive the two pulleys in a counterclockwise direction at room temperature (Figure 15b). The size of the

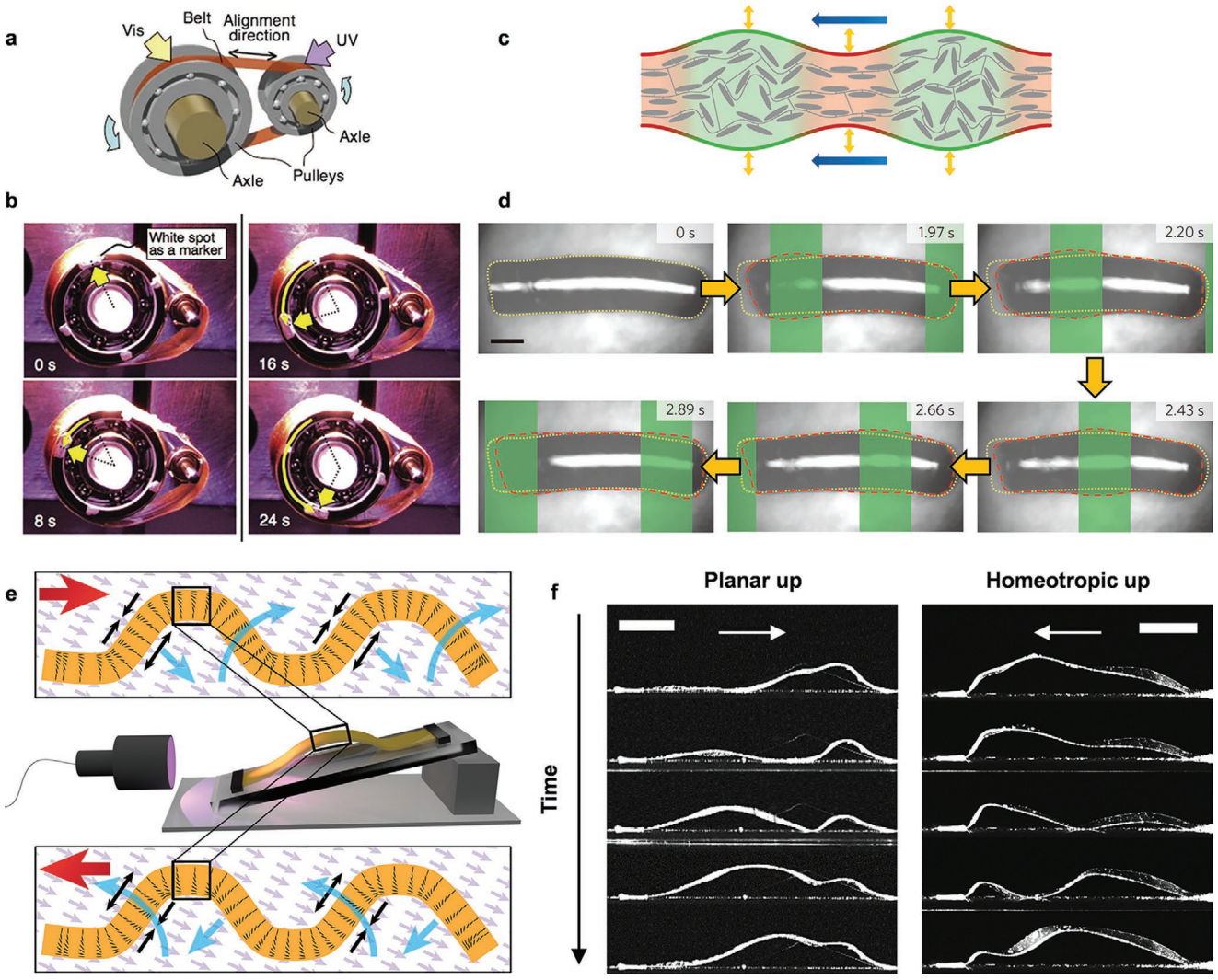

Figure 15. Self-sustainable motion. a) Schematic illustration of a photoinduced plastic motor system showing the relationship between light irradiation positions and a rotation direction. b) Series of photographs showing time profiles of the rotation of the photoinduced plastic motor with the CLCP laminated film induced by simultaneous irradiation with UV (366 nm, 240 mW cm^{-2}) and visible light (>500 nm, 120 mW cm^{-2}) at room temperature. Reproduced with permission.[69] Copyright 2008, Wiley-VCH. c) Concept of a selectively triggered continuous microrobot consisting of a soft active material. d) Experimental top-view images showing the deformation of an anchored cylindrical microrobot under a periodic light pattern travelling from left to right (illuminated area represented by the green overlay; first frame and yellow dotted line: rest configuration; red dashed line: deformed profile). Scale bar, 200 µm. Reproduced with permission.[80] Copyright 2016, Springer Nature. e) Schematic of the experimental set-up, showing a polymeric film that is constrained at both extremities under an oblique-incidence light source (left). The blue arrows show the way the film deforms while the red ones indicate the propagation direction of the wave. f) Comparison of experimental data for planar-up (left) and homeotropic-up (right) configurations. The arrows indicate the propagation direction of the wave. Scale bar, 5 mm. Reproduced with permission.[81] Copyright 2017, Springer Nature.

belt is in the range of millimeters for the demonstration, but is not in principle material-limited. Thus, numerous applications even on the nanoscale are possible, especially where efficient power supply to mechanical system is battery-free and noncontact.

Biological propulsion mechanisms are generally based on the common principle of travelling waves emerging from the distributed and self-coordinated action of many independent molecular motors (Figure 15c). To mimic this phenomenon, Fischer and co-workers showed self-propelled microrobots of photoactive azo-LCE, which performed versatile locomotion behaviors driven by structured monochromatic light.[80] Under irradiation of 532 nm light, both photochemical and photothermal effects simultaneously triggered the axial contraction and radial expansion of the planar aligned LCE cylinders. Therefore, when a binary periodic light filed travelling from left to right at a frequency of 1 Hz was projected onto the microrobot, the portions of the microrobot that are illuminated expanded transversely, and followed the projected pattern as it traveled along the body, resulting in continuous movement (Figure 15d). The directed motion of periodic light patterns drove deformation waves along the cylinder, so that drug the surrounding fluid and swam. The self-propulsion of the cylindrical microrobot by travelling-wave motions closely mimics the propulsion of microscopic biological swimmers,

particularly ciliates (for example, *Paramecium*) that self-propel using metachronal waves. The principle of using structured light could be extended to other applications that require microscale actuation with sophisticated spatiotemporal coordination for advanced microrobotic technologies.

An ingenious strategy for using an LCN to generate continuous, directional, macroscopic mechanical waves under constant light illumination, which were another form of dynamic motion added to the roster of LCN deformations, was reported by Broer, Selinger, and co-workers.[81] It is noted that the azobenzene derivatives that undergo fast thermal relaxation are key element in realizing continuous wave motion and are designed according to two principles: attaching a group that both pushes and pulls electrons on and off the azobenzene; or forming a tautomerizable azohydrazone. These azobenzene derivatives were incorporated into a splay-aligned LCN film, where the LC molecules were homeotropic at one surface and planar at the other. When the film was attached at both ends to a substrate within a distance shorter than the length of the strip, constant UV light exposure initiated a continuous millimeter-scale travelling wave that regenerates and propagates in a repeating, snake-like motion (Figure 15e,f). The wave propagation and regeneration are caused by self-shadowing of the film—continuous displacement of the wave changes the position of the areas exposed to and hidden from the UV irradiation, and these variations generate feedback that drives the waves. Furthermore, the direction of the waves was controlled by the alignment of the planar and homeotropic sides of the film with respect to the UV irradiation, because each side responds differently to the irradiation. Interestingly, they demonstrated that the sand placed on the film was continuously transported and was even thrown far from the film, if there is a sudden release of energy. The film was also used to carry uphill an object that was much heavier and larger than the film itself. It is anticipated that the generation of waves has potential applications in the fields of photomechanical energy harvesting, self-cleaning surfaces, and miniaturized robots.

4.4. Self-Regulation

Mimicking the natural intelligence to devise tiny systems that are capable of self-regulated action gains most interests but remains among the grand challenges in biomimetic microrobotics.[82] Priimagi, Zeng, and co-workers demonstrated an intelligent gripping device, a splay-aligned LCE doped with photothermal agent (Disperse Red 1), which is capable of mimicking the motions of natural flytrap (*Dionaea muscipula*), by performing autonomous closure action (gripping) and self-recognition between different microobjects through sensing their physical properties.[83] The LCE was integrated onto the tip of an optical fiber (attached to the homeotropically aligned surface), leaving a transparent window in the center. A 488 nm laser (200 mW) was coupled to the other end of the fiber, and emitted through the center of the device. When an object entered into the field of view and produced enough optical feedback (reflected/scattered light), the LCE bent toward the object (closure action), eventually capturing it (**Figure 16**a). Moreover, the optical feedback was determined by the reflectance/scattering intensity of the object, so that the device can obtain autonomous recognition and distinction between different microobjects.

Inspired by heliotropism in leaves or flowers, Jiang and coworkers realized artificial heliotropism for solar cells, utilizing actuators based on a photo-thermomechanical fiber-network/SWNT/LCE nanocomposite, where the polyurethane fiber-networks was used as the reinforcement phase for the uniaxially planar aligned nematic LCE matrices to improve mechanical property.[84] The solar cells were installed on a platform that was connected to actuators and elastically supported so that it can tile under the actuation force (Figure 16b). At any time,

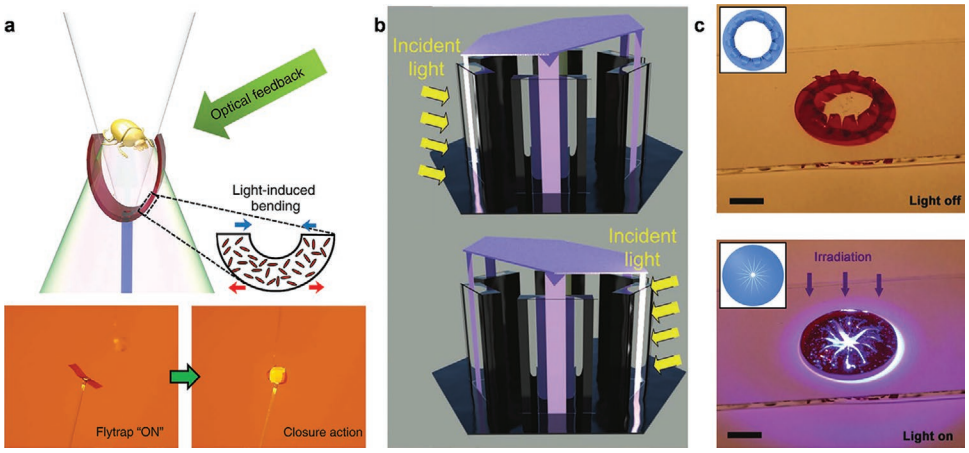

Figure 16. Self-regulation. a) The flytrap closes when an object enters its field of view and causes optical feedback to the LCE actuator. Light-induced bending of the LCE leads to closure action, thus capturing the object (top). The optical flytrap mimics the motion of a natural flytrap by capturing a small scattering object falling on the gripper (bottom). Reproduced with permission.[83] Copyright 2017, Springer Nature. b) 3D schematic of the heliotropic behavior. The actuator(s) facing the sun contracts, tilting the solar cell toward the sunlight. Reproduced with permission.[84] Copyright 2012, Wiley-VCH. c) Soft LCE iris in the open state when no light impinges on it (top) and the iris closes upon light illumination (470 nm, 250 mW cm^{-2}) (bottom). Scale bar, 5 mm. Inset: schematic drawing of the light-driven iris at its closed state, where light illumination triggers petal segments to bend inward and to reduce the aperture size. The iris is open under weak/no light conditions, when the anisotropic thermal expansion induces bending in the segments, thus opening the aperture. Reproduced with permission.[85] Copyright 2017, Wiley-VCH.

actuators facing the incoming sunlight would be in a contracted state, while other actuators not exposed to the sunlight would be in the relaxed state, tilting the solar cells toward the sun. This artificial heliotropism had a 60° of range in altitude angle, and 180° of range in azimuth angle, and significant increase in the output photocurrent of the solar cells was observed.

In the human iris, the sphincter and dilator muscles control the pupil size in order to stabilize the light transmission into the retina. Priimagi, Zeng, and co-workers reported an iris-like LCE device that can perform automatic shape-adjustment by reacting to the incident light power density.[85] The photothermal LCE device was composed of 12 radially splay-aligned segments prepared by photoalignment technique. By employing anisotropic thermal expansion within the polymerized LCE, the iris was initially in the open state under low-light conditions. When uniformly irradiated with 470 nm light (250 mW cm^{-2}), all the iris segments bent inward and the aperture closed (Figure 16c).

By mimicking coral polyps that induce currents through coordinated motion to attract and capture suspended targets in marine environments, Schenning, Toonder, and co-workers demonstrated an artificial aquatic gripper capable of generating fluid flow and grasping suspended objects.[86] The gripper is composed of a magnetic responsive flexible polydimethylsiloxane stem and two photoresponsive planar aligned LCN grasping arms. In the process, the aquatic gripper firstly created a general spiraling fluid flow directed toward itself under rotated magnetic field to attract suspend objects. And then upon 365 nm UV irradiation (<40 mW cm^{-2}), the azobenzene-doped LCN grasping arms bent toward the light owing to the strain gradient induced by photochemical phase transition, and captured the objects. The reverse opening actuation and release of the object was triggered by irradiation of 455 nm blue light.

4.5. Liquid Manipulation

Microfluidics generally refers to technologies using microfabricated structures to precisely manipulate fluids at the microscale or smaller. Conversion of light energy to liquid motion is a new paradigm for the actuation of microfluidic systems by using light-induced capillary forces. Yu and co-workers presented a conceptually novel way to propel liquids by capillary force arising from photoinduced asymmetric deformation of tubular microactuators (TMAs), which relies on neither wettability gradients nor the Marangoni effect.[30] Inspired by the skill of long-billed birds that small amounts of liquids are propelled by changing shapes of droplets through small-angle opening and closing of bills,[87] the TMAs were designed to deform from cylindrical to conical shape upon exposure to attenuated 470 nm light (**Figure 17**a). First, the TMAs were fabricated by using the novel azobenzene-containing LLCP with high molecular weight and enough mechanical robustness in the absence of chemical crosslinks. Second, the photoinduced reorientation of azobenzene mesogens in lamellar structures under 470 nm light triggered the geometric change of the TMA from cylindrical to conical shape, which generated Laplace pressure difference (asymmetric capillary force) for liquid propulsion toward the light attenuated direction. These microactuators were able to exert photocontrol of a wide diversity of liquids over a long distance with controllable velocity and direction (Figure 17b), including not only simple liquids spanning from nonpolar to polar liquids, but also complex fluids used in biochemical engineering, such as bovine serum albumin solution, phosphate buffer solution, and cell culture medium. The propelling speed of a liquid in the TMA reached up to 5.9 mm s^{-1}, and the moving distance reached 57 mm, which were the highest records of liquid motion driven by light-induced capillary force so far. Notably, without any auxiliary units, the TMAs were capable of mixing multiple liquids, accelerating dissolution of the solutes, capturing microspheres on the microscale, and even making liquids run uphill. Therefore, the photodeformable TMAs offer a versatile toolbox and are promising candidates for applications in the fields of microreactors, laboratory-on-a-chip settings, and micro-optomechanical systems.

Recently, Yu and co-workers further developed bilayer photocontrollable flexible microtubes (PFMs) composed of a photodeformable LLCP layer and an outer flexible EVA supporting layer, which were able to propel various liquids in the predetermined direction.[31a] The photoreorientation of the azobenzene mesogens in the lamellar structure of LLCP layer induced the shape change of the whole microtube from cylindrical to conical, consequently generating the asymmetric capillary force. The supporting EVA layer provided elasticity for tight connection between PFM themselves or other microtubes. Based on this feature, a closed-loop microfluidic actuator was fabricated by end-to-end connection of one single PFM, where the confined isopropanol slug was propelled counterclockwise. Furthermore, light-directed liquid motion in the PFM attached to a finger was demonstrated as an example of potential wearable devices. Under the 470 nm light (80 mW cm^{-2}), the liquid slug was manipulated away from or close to the fingertip in both straight and curved states (Figure 17c). Such feature was attributed to the bilayer structure of the PFM that was capable of being changed into arbitrary 3D shapes (trajectories) to propel the inner liquids by photodeformation. In addition, the photoinduced self-healing property of the PFMs enhanced their reliability in applications of wearable and integrated microfluidic systems. These unique PFMs would find use in microelectromechanical systems and lab-on-a-chip settings as the photocontrollable components and liquid manipulation tools.

In addition to the microchannels, manipulating small water droplets on an open, intelligent surface with tunable wettability has attracted considerable interests because of potential applications ranging from no-loss transfer to surface chemistry.[88] However, few of the previously reported researches involved a method to fabricate intelligent surfaces with photoswitchable superhydrophobic adhesion. Yu and co-workers reported a light-regulated adhesion switch on a microarrayed CLCP superhydrophobic surface fabricated by polydimethylsiloxane-soft-template-based secondary replication.[89] After 365 nm UV light irradiation, the sliding angle of the CLCP film increased from 67.7° to 90° since the dipole moment of *cis* isomers led to the increase of local polarity of polymer chain. Subsequently, the surface reverted to lower adhesive state after 530 nm visible light irradiation. Such a quick (<1 min) and reversible switch of superhydrophobic adhesion retained well after many cycles of alternative irradiation of UV and visible light. Besides, they also fabricated CLCP films with

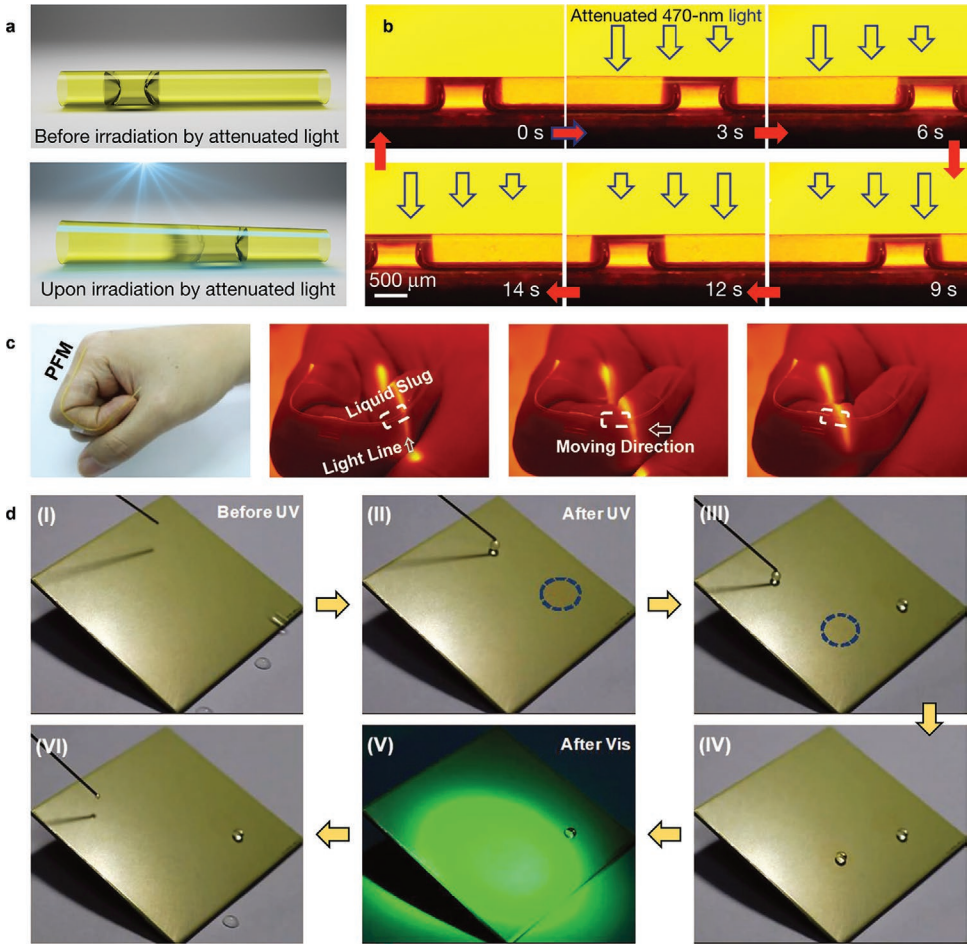

Figure 17. Liquid manipulation. a) Schematics showing the motion of a slug of fully wetting liquid confined in a tubular microactuator (TMA) driven by photodeformation. b) Lateral photographs of the light-induced motion of a silicone oil slug in a TMA fixed on a substrate. On irradiation by 470 nm light whose intensity is attenuated increasingly from left to right (top row), the silicone oil slug is self-propelled toward the right; when the direction of attenuation is reversed (bottom row), the direction of movement of the slug is also reversed. Reproduced with permission.[30] Copyright 2016, Springer Nature. c) Photocontrolled transport of an isopropanol slug in the PFM attached on the index finger upon the irradiation of 470 nm line light (80 mW cm^{-2}). Reproduced with permission.[31a] Copyright 2019, Wiley-VCH. d) Photographs of directed pinning of moving water droplets on superhydrophobic mat: i) 8 μL water droplets rolling down the surface of the mat; ii–iv) the circled areas are shined by UV light, turning orange owing to the photoisomerization of azobenzene units. Then, the moving droplets could be pinned at the UV-irradiated points; v,vi) the mat returns to a low AF state after visible light irradiation and the droplets slid down smoothly. UV light: 365 nm, 20 mW cm^{-2}; visible light: 530 nm, 60 mW cm^{-2}; size of the mat: 5.0 cm × 5.0 cm. Reproduced with permission.[91] Copyright 2019, Wiley-VCH.

different surface topographies, including sub-micropillar and sub-microcone arrays, through colloidal lithography technique by modulating different types of etching masks. Interestingly, these two films of the same chemical structure represented completely different wetting state of water adhesion, which mimicked the high adhesive rose petals and low adhesive lotus leaves, respectively.[90]

Electrospinning has advantages in directly and continuously fabricating superhydrophobic nanofiber mats with unique surface roughness and texture in a large scale. However, this technology is not compatible to the CLCPs. Yu and co-workers presented photoresponsive superhydrophobic mats fabricated by the electrospinning of the LLCP with high molecular weight.[91] After 365 nm UV irradiation, the LLCP mat retained superhydrophobic state, whereas the adhesive force of the mat was enlarged by 100% compared to that at the initial state. The rapid and large variation in adhesive force and the surface free energy on the mats arose from the polarity change and the reorientation of the azobenzene mesogens in nanofibers. The water droplets were pinned at any point on the mat surface after the rapid switch of superhydrophobic adhesion triggered by the remote light control. Notably, the directed pinning of moving water droplets was achieved on the inclined LLCP mat (Figure 17d). At the initial state, the water droplets rolled down the inclined superhydrophobic surface with a slant angle of 20°. After UV light irradiation, the moving water droplets were pinned by the exposed area due to the increased adhesive force. After removing the pinned droplets and irradiated by visible light, the irradiated area returned to a low adhesion state and thus the new droplets could roll down again. It is expected that the active manipulation of discrete droplets on an open surface by using such photoresponsive mats provides a new concept for microdroplet manipulation, allowing for minimal reactions among biological samples.

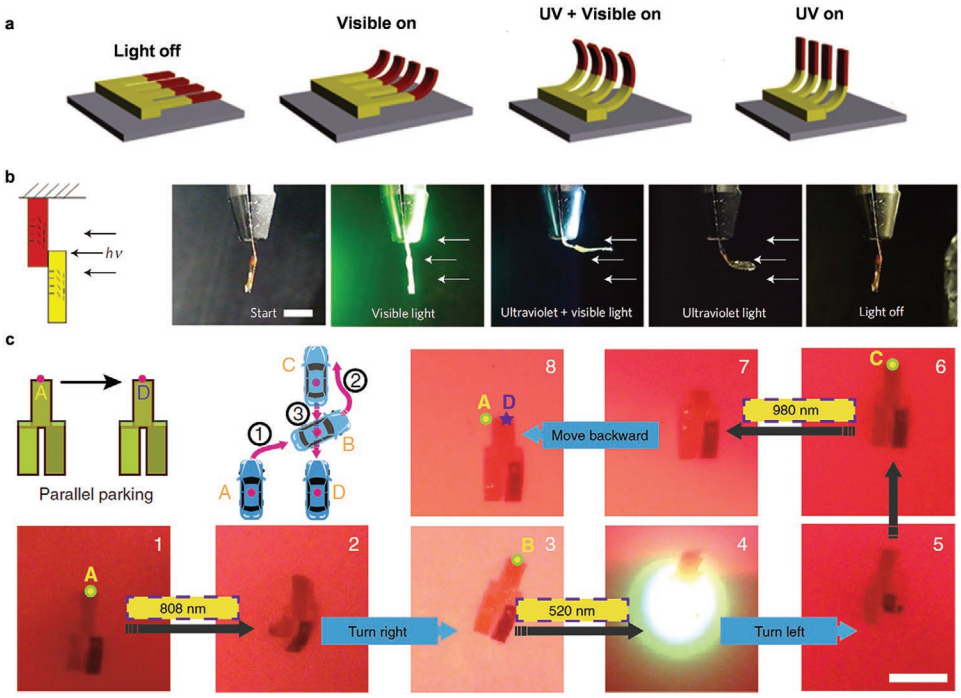

Figure 18. a) Artificial, light-driven cilia produce an asymmetric motion controlled by the spectral composition of the light. b) Schematic representation of the macroscopic set-up showing the orientation of the molecules and steady-state responses of a modular LCN actuator (10 µm thick, 3 mm wide, 10 mm long) to different colors of light. Scale bar, 5 mm. Reproduced with permission.[93] Copyright 2009, Springer Nature. c) Photoguided parallel parking of LCE walker robot. Photographs showing the process of such a vehicle-like walker robot moving horizontally from position A to position D under the stimulation of 808, 520, and 980 nm light. Scale bar, 1 cm. Reproduced with permission.[94] Copyright 2019, Springer Nature.

4.6. Multiwavelength-Responsive Actuation

The majority of light-fueled soft actuators are based on single actuation mode, while complex multifunctionality or multitasking is rarely presented but increasingly needed. The integrated actuators working in concert to perform tasks will realize orchestrated motions. Such assemblies typically contain various soft actuators of different materials in response to light stimuli with different wavelengths.[41,92] van Oosten and co-workers used inkjet printing technology to create cilia-like LCN actuators with two kinds of azobenzene dyes in different subunits, which were selectively addressed by various light.[93] Under exposure to 445–550 nm light (4 mW cm^{-2}), the top part with visible light-sensitive azobenzene dyes bent because of photochemical isomerization, whereas the UV light-sensitive bottom part with the other azobenzene dye bent upon 365 nm light (9 mW cm^{-2}) irradiation (**Figure 18**a,b). By modulating the asymmetric motions of the cilia-like actuators at few hertz, effective fluid manipulation in microsystems could be realized.

Based on three photothermal agents with noninterfered absorptions, Yang and co-workers built a multistimuli-responsive vehicle-like LCE walker robot.[94] A parallel parking motion of the walker robot with three legs was demonstrated by selectively stimulating one of the legs with different wavelengths of light (Figure 18c). Under the stimulation of 808 nm NIR light (0.18 W cm^{-2}), only the temperature of the left leg rose to above the LC-isotropic transition (74.5 °C), inducing asymmetric downward bending of the planar-aligned film and forcing the robot to turn right. Then under the irradiation of 520 nm green light (47 mW cm^{-2}), the right leg deformed so that the robot moves left, followed by irradiating with 980 nm NIR light (0.19 W cm^{-2}) to reverse backward.

Moreover, Yang and co-workers combined shape-morphing and color-changing capability into a bilayered LCE film, which possess trilight-modulated properties.[95] The bottom layer of the LCE film was incorporated with a NIR absorbing dye as photothermal agents, whereas the planar-aligned upper layer was prepared based on two spiropyran derivatives. When exposed to 808 nm NIR light (0.83 W cm^{-2}), the film bent toward the light due to the photothermal-induced asymmetric shrinkage, and the color changed to red brown. In the irradiation of 520 visible light or 365 nm UV light, only the color of the film changed between green and murrey.

5. Conclusion

Photodeformable LCPs, which exhibit large macroscopic shape changes, are envisioned to bring new functionality and drive innovation in the fields of soft robotics, solar-energy harvesting, and microfluidics. The ability of LCPs to self-organize to form materials of homogeneous composition with spatial variation of the mechanical response is not simple to emulate in other stimuli-responsive materials. The main strategies to construct LCP actuators include modulating the director fields of LCPs and designing novel materials. The complicated director fields of the LCs give rise to unique actuating behavior. Based on different surface-alignment methods (rubbing, magnetic fields, and photoalignment), various hierarchical alignment in LCP

materials is involved, from simple planar, topological defect structures to complex patterned alignment. According to the mobility and automation, the actuation of the LCPs is classified into different categories. The actuators require temporal modulation controlled by spatially uniform light, e.g., scanned or structured laser beams, which is used to induce locomotion including the crawling caterpillar and miniature swimmer. Oscillation is realized by alternatively exposing and shielding the actuators to stationary light fields. In this process, the actuators transfer the energy absorbed from external laser to continuous periodic motion. For self-sustainable actuators, more complex motions are demonstrated under constant illumination of light. Self-regulation is related to the actuators interacted with the environment, joining efforts to autonomously execute sophisticated tasks.

The materials, alignment, mechanisms, and light sources in different light-fueled actuation are summarized in **Table 2**. The evolution trends of generating light-fueled LCP soft actuators mainly involves in three aspects. First, although multifunctional actuators are manipulated via programmable and sophisticated shape change, most of the actuation is an integration of the basic bending mode, which is combined with ingenious design of geometries of actuators (for example, asymmetric film for walking, spiral ribbons or origami geometries for rolling and disc for swimming) or structured light fields with different frequency or patterns. Therefore, the planar or splayed alignment, determining the bending deformation due to the different degrees of contraction or expansion, is frequently employed to create multifunctional actuators. Second, the wavelength of light triggering deformation depends on the photoresponsive units. Photochemical phase transition is extensively based on *trans-cis* photoisomerization of azobenzenes induced by UV light, and long conjugated azotolanes as well as UCL technology have been developed to extend the wavelength to cover visible even NIR region. In the case of photothermal effect, photothermal agents have different maximum absorption, hence light of wavelengths from UV to NIR could also be selected. Third, mechanical properties provided by the LCPs should be taken into consideration according to the functionality of actuators. For example, most self-oscillations are

Table 2. Summary of the materials, mechanisms, and light sources in different light-fueled actuation.

Actuation	Materials	Phases	Alignment	Mechanisms[a)]	Light sources	Ref.
Locomotion	Azo dye-LCE	Nematic	Planar	Photothermal	532 nm (10 W mm^{-2})	[68]
	Disperse Orange 3/LCE	Nematic	Planar	Photothermal	532 nm (5.5 W)	[66]
	Azo-CLCP	Smectic	Planar	Photochemical	366 nm (240 mW cm^{-2}) >540 nm (120 mW cm^{-2})	[64]
	Disperse Red 1/LCE	Nematic	Splayed	Photothermal	488 nm (220 mW cm^{-2})	[67]
	SWNT/LCE	Nematic	Planar	Photothermal	980 nm (28.2 mW mm^{-2})	[65]
	Azo-LCN	Nematic	Twisted	Photochemical Photothermal	320–500 nm (200 mW mm^{-2})	[70]
	Disperse Red 1/LCN	–	Splayed	Photothermal	470 nm (320 mW cm^{-2})	[71]
Oscillation	Azo-LCN	Nematic	Planar	Weigert	442 nm (0.8–1.5 W cm^{-2})	[74–76]
	Dye[a)]/LCN	–	Splayed	Photothermal	365 nm (0.52 W cm^{-2})	[78]
	Fazo[b)]-LCN	–	Splayed	Photochemical	405 nm (157 mW cm^{-2}) 530 nm (318.8 mW cm^{-2}) Sunlight	[77]
	PDA/LCN	–	Splayed	Photothermal	808 nm (2.1 W cm^{-2})	[79]
Self-sustainable motion	Azo-LCE/PE	Smectic	Planar	Photochemical	366 nm (200 mW cm^{-2}) >500 nm (120 mW cm^{-2})	[69]
	Azo-LCN	–	Splayed	Photothermal	405 nm (510 mW cm^{-2})	[81]
	Azo-LCE	Nematic	Planar	Photochemical Photothermal	532 nm (structured light)	[80]
Self-regulation	Disperse Red 1/LCE	–	Splayed	Photothermal	488 nm (200 mW)	[83]
	Disperse Red 1/LCE	–	Splayed	Photothermal	470 nm (250 mW cm^{-2})	[85]
	SWNT/LCE	Nematic	Planar	Photothermal	White light (230 mW cm^{-2})	[84]
Liquid manipulation	Azo-LLCP	Smectic	Out-plane	Weigert	470 nm (125–140 mW cm^{-2})	[30]
	Azo-LLCP/EVA	Smectic	Out-plane	Weigert	470 nm (80 or 120 mW cm^{-2})	[31a]
	Azo-LLCP	Smectic	–	Photochemical	365 nm (20 mW cm^{-2}) 530 nm (60 mW cm^{-2})	[91]
	Azo-CLCP	Nematic	Planar	Photochemical	365 nm (120 mW cm^{-2}) 530 nm (30 mW cm^{-2})	[89]
	Azotolane-CLCP	Nematic	Planar	Photochemical	470 nm (120 mW cm^{-2}) 530 nm (30 mW cm^{-2})	[90]

[a)]Dye: (hydroxyphenyl)benzotriazoles; [b)]F-azo: *ortho*-fluoroazobenzene dye.

realized based on the LCNs with densely crosslinking density, where superior elastic properties are required to bring the films to the intital position rapidly after light irradiation.

Significant progress has been made in designing faster actuating materials with better shape control and superior mechanical stability. However, many of the challenges faced by the photodeformable LCPs have not been adequately addressed. First, most of the reported light-fueled actuators are limited to thin films or thin rods of material, which confines the field of light-fueled actuation to superficial applications required minimal mechanical force and motion range.[3b] Second, material fatigue is a major problem of the actuators. Reliable performance for thousands, millions, or even billions of cycles is expected from practical devices, many times more than what has been currently achieved in the LCP actuators. Moreover, only a minimal number of suitable photochemical reactions discovered so far may be one limitation in the photoinduced actuation of the LCPs. As a result, further research efforts should be urgently concentrated in designing photoresponsive LCPs with new photochrome molecules. Importantly, the energy transfer efficiency from light to mechanical work is relatively low at the current stage, which inevitably limits practical applications of light-fueled LCP actuators and needs to be addressed stepwise by researchers in the near future. The aim of the light-fueled LCP-based soft actuators is to simplify the required control strategy and increase the functionality at the same time.

Acknowledgements

This work was financially supported by the National Natural Science Foundation of China (Grant Nos. 21734003, 51927805, and 51721002), National Key R&D Program of China (2016YFA0202902 and 2017YFA0701302), and Innovation Program of Shanghai Municipal Education Commission (2017-01-07-00-07-E00027). This article is part of the *Advanced Optical Materials* Hall of Fame article series, which recognizes the excellent contributions of leading researchers to the field of optical materials science.

Conflict of Interest

The authors declare no conflict of interest.

Keywords

actuators, liquid crystal polymers, photochemical phase transition, photodeformation, photothermal effect

Received: October 10, 2020
Revised: January 9, 2021
Published online:

[1] K. Oliver, A. Seddon, R. S. Trask, *J. Mater. Sci.* **2016**, *51*, 10663.
[2] a) Y. Shang, J. Wang, T. Ikeda, L. Jiang, *J. Mater. Chem. C* **2019**, *7*, 3413; b) H. K. Bisoyi, Q. Li, *Chem. Rev.* **2016**, *116*, 15089; c) Y. Yu, T. Ikeda, *Angew. Chem.* **2006**, *45*, 5416; d) W. Gu, J. Wei, Y. Yu, *Chin. Phys. B* **2016**, *25*, 096103.
[3] a) T. J. White, D. J. Broer, *Nat. Mater.* **2015**, *14*, 1087; b) G. Stoychev, A. Kirillova, L. Ionov, *Adv. Opt. Mater.* **2019**, *7*, 1900067; c) T. J. White, *J. Polym. Sci., Part B: Polym. Phys.* **2018**, *56*, 695.
[4] a) F. Ge, Y. Zhao, *Adv. Funct. Mater.* **2019**, *30*, 1901890; b) H. Koerner, T. J. White, N. V. Tabiryan, T. J. Bunning, R. A. Vaia, *Mater. Today* **2008**, *11*, 34; c) Z. Wang, H. Q. Zhang, *Chin. J. Polym. Sci.* **2020**, *38*, 37.
[5] a) Y. Yu, T. Ikeda, *Macromol. Chem. Phys.* **2005**, *206*, 1705; b) T. Ikeda, T. Ube, *Mater. Today* **2011**, *14*, 480.
[6] a) X. Pang, J.-a. Lv, C. Zhu, L. Qin, Y. Yu, *Adv. Mater.* **2019**, *31*, 1904224; b) T. Ube, T. Ikeda, *Adv. Opt. Mater.* **2019**, *7*, 1900380; c) T. Ikeda, J. Mamiya, Y. Yu, *Angew. Chem.* **2007**, *46*, 506; d) T. Ube, T. Ikeda, *Angew. Chem.* **2014**, *53*, 10290; e) W. Gu, X. Qing, J. Wei, Y. Yu, *Chin. Sci. Bull.* **2016**, *61*, 2102; f) H. Yu, *J. Mater. Chem. C* **2014**, *2*, 3047; g) J. Wei, Y. Yu, *Soft Matter* **2012**, *8*, 8050; h) X. Qing, J.-a. Lv, Y. Yu, *Acta Polym. Sin.* **2017**, *11*, 1679; i) T. J. White, *Photomechanical Materials, Composites, and Systems: Wireless Transduction of Light into Work*, Wiley, Hoboken, NJ **2017**.
[7] X. Qing, L. Qin, W. Gu, Y. Yu, *Liq. Cryst.* **2016**, *43*, 2114.
[8] P. G. de Gennes, M. Hébert, R. Kant, *Macromol. Symp.* **1997**, *113*, 39.
[9] a) G. Vantomme, A. H. Gelebart, D. J. Broer, E. W. Meijer, *Tetrahedron* **2017**, *73*, 4963; b) D. Liu, C. W. Bastiaansen, J. M. den Toonder, D. J. Broer, *Angew. Chem.* **2012**, *51*, 892; c) D. Liu, D. J. Broer, *Angew. Chem.* **2014**, *53*, 4542; d) A. H. Gelebart, M. Mc Bride, A. P. H. J. Schenning, C. N. Bowman, D. J. Broer, *Adv. Funct. Mater.* **2016**, *26*, 5322; e) T. Ube, K. Kawasaki, T. Ikeda, *Adv. Mater.* **2016**, *28*, 8212; f) B. R. Donovan, V. M. Matavulj, S. K. Ahn, T. Guin, T. J. White, *Adv. Mater.* **2019**, *31*, 1805750; g) X. Pang, B. Xu, X. Qing, J. Wei, Y. Yu, *Macromol. Rapid Commun.* **2018**, *39*, 1700237; h) Y. Liu, B. Xu, S. Sun, J. Wei, L. Wu, Y. Yu, *Adv. Mater.* **2017**, *29*, 1604792.
[10] a) E. K. Fleischmann, R. Zentel, *Angew. Chem.* **2013**, *52*, 8810; b) C. J. Barrett, J.-i. Mamiya, K. G. Yager, T. Ikeda, *Soft Matter* **2007**, *3*, 1249.
[11] H. Finkelmann, E. Nishikawa, G. G. Pereira, M. Warner, *Phys. Rev. Lett.* **2001**, *87*, 015501.
[12] M. H. Li, P. Keller, B. Li, X. G. Wang, M. Brunet, *Adv. Mater.* **2003**, *15*, 569.
[13] a) T. Ikeda, M. Nakano, Y. Yu, O. Tsutsumi, A. Kanazawa, *Adv. Mater.* **2003**, *15*, 201; b) T. Yoshino, M. Kondo, J. Mamiya, M. Kinoshita, Y. Yu, T. Ikeda, *Adv. Mater.* **2010**, *22*, 1361.
[14] Y. Yu, T. Maeda, J.-i. Mamiya, T. Ikeda, *Angew. Chem.* **2007**, *119*, 899.
[15] a) Y. Yu, M. Nakano, A. Shishido, T. Shiono, T. Ikeda, *Chem. Mater.* **2004**, *16*, 1637; b) J. Garcia-Amoros, H. Finkelmann, D. Velasco, *J. Mater. Chem.* **2011**, *21*, 1094.
[16] Y. Zhang, J. Xu, F. Cheng, R. Yin, C.-C. Yen, Y. Yu, *J. Mater. Chem.* **2010**, *20*, 7123.
[17] M. Kondo, M. Sugimoto, M. Yamada, Y. Naka, J.-i. Mamiya, M. Kinoshita, A. Shishido, Y. Yu, T. Ikeda, *J. Mater. Chem.* **2010**, *20*, 117.
[18] A. Priimagi, A. Shimamura, M. Kondo, T. Hiraoka, S. Kubo, J.-I. Mamiya, M. Kinoshita, T. Ikeda, A. Shishido, *ACS Macro Lett.* **2012**, *1*, 96.
[19] A. H. Gelebart, M. M. Bride, A. P. H. J. Schenning, C. N. Bowman, D. J. Broer, *Adv. Funct. Mater.* **2016**, *26*, 5322.
[20] L. Liu, M. del Pozo, F. Moheninejad, M. G. Debije, D. J. Broer, A. P. H. J. Schenning, *Adv. Opt. Mater.* **2020**, *8*, 2000732.
[21] A. Ryabchun, Q. Li, F. Lancia, I. Aprahamian, N. Katsonis, *J. Am. Chem. Soc.* **2019**, *141*, 1196.
[22] F. Cheng, Y. Zhang, R. Yin, Y. Yu, *J. Mater. Chem.* **2010**, *20*, 4888.
[23] R. Yin, W. Xu, M. Kondo, C. C. Yen, J.-i. Mamiya, T. Ikeda, Y. Yu, *J. Mater. Chem.* **2009**, *19*, 3141.
[24] F. Cheng, R. Yin, Y. Zhang, C.-C. Yen, Y. Yu, *Soft Matter* **2010**, *6*, 3447.
[25] Z. Jiang, M. Xu, F. Li, Y. Yu, *J. Am. Chem. Soc.* **2013**, *135*, 16446.
[26] W. Wu, L. Yao, T. Yang, R. Yin, F. Li, Y. Yu, *J. Am. Chem. Soc.* **2011**, *133*, 15810.
[27] Y. Yu, M. Nakano, T. Ikeda, *Nature* **2003**, *425*, 145.

[28] a) S. L. Oscurato, M. Salvatore, P. Maddalena, A. Ambrosio, *Nanophotonics* **2018**, *7*, 1387; b) T. Ikeda, *J. Mater. Chem.* **2003**, *13*, 2037.
[29] N. Tabiryan, S. Serak, X.-M. Dai, T. Bunning, *Opt. Express* **2005**, *13*, 7442.
[30] J.-a. Lv, Y. Liu, J. Wei, E. Chen, L. Qin, Y. Yu, *Nature* **2016**, *537*, 179.
[31] a) B. Xu, C. Zhu, L. Qin, J. Wei, Y. Yu, *Small* **2019**, *15*, 1901847; b) S. Q. Han, Y. Y. Chen, B. Xu, J. Wei, Y. Yu, *Chin. J. Polym. Sci.* **2020**, *38*, 806; c) X. Qing, Y. Liu, J. Wei, R. Zheng, C. Zhu, Y. Yu, *Adv. Opt. Mater.* **2018**, *7*, 1801494; d) Q. Liu, Y. Liu, J.-a. Lv, E. Chen, Y. Yu, *Adv. Intell. Syst.* **2019**, *1*, 1900060; e) X. Pang, L. Qin, B. Xu, Q. Liu, Y. Yu, *Adv. Funct. Mater.* **2020**, *30*, 2002451.
[32] a) C. Ohm, M. Brehmer, R. Zentel, *Adv. Mater.* **2010**, *22*, 3366; b) E. K. Fleischmann, H. L. Liang, N. Kapernaum, F. Giesselmann, J. Lagerwall, R. Zentel, *Nat. Commun.* **2012**, *3*, 1178; c) A. Resetic, J. Milavec, B. Zupancic, V. Domenici, B. Zalar, *Nat. Commun.* **2016**, *7*, 13140; d) Z. Pei, Y. Yang, Q. Chen, E. M. Terentjev, Y. Wei, Y. Ji, *Nat. Mater.* **2014**, *13*, 36; e) Y. Zhang, Z. Wang, Y. Yang, Q. Chen, X. Qian, Y. Wu, H. Liang, Y. Xu, Y. Wei, Y. Ji, *Sci. Adv.* **2020**, *6*, eaay8606; f) H. Aharoni, Y. Xia, X. Zhang, R. D. Kamien, S. Yang, *Proc. Natl. Acad. Sci. USA* **2018**, *115*, 7206; g) H. Shahsavan, S. M. Salili, A. Jakli, B. Zhao, *Adv. Mater.* **2015**, *27*, 6828; h) K. M. Lee, T. J. Bunning, T. J. White, *Adv. Mater.* **2012**, *24*, 2839.
[33] a) L. Dong, Y. Zhao, *Mater. Chem. Front.* **2018**, *2*, 1932; b) Z. C. Jiang, Y. Y. Xiao, Y. Zhao, *Adv. Opt. Mater.* **2019**, *7*, 1900262; c) H. K. Bisoyi, A. M. Urbas, Q. Li, *Adv. Opt. Mater.* **2018**, *6*, 1800458.
[34] L. Yang, K. Setyowati, A. Li, S. Gong, J. Chen, *Adv. Mater.* **2008**, *20*, 2271.
[35] A. H. Gelebart, D. J. Mulder, G. Vantomme, A. Schenning, D. J. Broer, *Angew. Chem.* **2017**, *56*, 13436.
[36] M. Lahikainen, K. Kuntze, H. Zeng, S. Helantera, S. Hecht, A. Priimagi, *ACS Appl. Mater. Interfaces* **2020**, *12*, 47939.
[37] R. Lan, J. Sun, C. Shen, R. Huang, Z. Zhang, C. Ma, J. Bao, L. Zhang, L. Wang, D. Yang, H. Yang, *Adv. Funct. Mater.* **2020**, *30*, 2000252.
[38] X. Liu, R. Wei, P. T. Hoang, X. Wang, T. Liu, P. Keller, *Adv. Funct. Mater.* **2015**, *25*, 3022.
[39] Z. Li, Y. Yang, Z. Wang, X. Zhang, Q. Chen, X. Qian, N. Liu, Y. Wei, Y. Ji, *J. Mater. Chem. A* **2017**, *5*, 6740.
[40] L. Liu, M. H. Liu, L. L. Deng, B. P. Lin, H. Yang, *J. Am. Chem. Soc.* **2017**, *139*, 11333.
[41] M. P. da Cunha, M. G. Debije, A. P. H. J. Schenning, *Chem. Soc. Rev.* **2020**, *49*, 6568.
[42] M. P. da Cunha, E. A. J. van Thoor, M. G. Debije, D. J. Broer, A. P. H. J. Schenning, *J. Mater. Chem. C* **2019**, *7*, 13502.
[43] a) H. Kim, J. A. Lee, C. P. Ambulo, H. B. Lee, S. H. Kim, V. V. Naik, C. S. Haines, A. E. Aliev, R. Ovalle-Robles, R. H. Baughman, T. H. Ware, *Adv. Funct. Mater.* **2019**, *29*, 1905063; b) Q. Liu, Y. Zhan, J. Wei, W. Ji, W. Hu, Y. Yu, *Soft Matter* **2017**, *13*, 6145; c) L. T. de Haan, A. P. H. J. Schenning, D. J. Broer, *Polymer* **2014**, *55*, 5885; d) O. M. Wani, H. Zeng, P. Wasylczyk, A. Priimagi, *Adv. Opt. Mater.* **2018**, *6*, 1700949.
[44] Y. Yu, T. Ikeda, *J. Photochem. Photobiol., C* **2004**, *5*, 247.
[45] M. Kondo, Y. Yu, T. Ikeda, *Angew. Chem.* **2006**, *118*, 1406.
[46] a) M. Wang, B. P. Lin, H. Yang, *Nat. Commun.* **2016**, *7*, 13981; b) A. Priimagi, C. J. Barrett, A. Shishido, *J. Mater. Chem. C* **2014**, *2*, 7155.
[47] K. D. Harris, R. Cuypers, P. Scheibe, C. L. van Oosten, C. W. M. Bastiaansen, J. Lub, D. J. Broer, *J. Mater. Chem.* **2005**, *15*, 5043.
[48] S. Iamsaard, S. J. Aßhoff, B. Matt, T. Kudernac, J. J. L. M. Cornelissen, S. P. Fletcher, N. Katsonis, *Nat. Chem.* **2014**, *6*, 229.
[49] S. Iamsaard, E. Anger, S. J. Asshoff, A. Depauw, S. P. Fletcher, N. Katsonis, *Angew. Chem.* **2016**, *55*, 9908.
[50] S. Armon, E. Efrati, R. Kupferman, E. Sharon, *Science* **2011**, *333*, 1726.
[51] S. J. Asshoff, F. Lancia, S. Iamsaard, B. Matt, T. Kudernac, S. P. Fletcher, N. Katsonis, *Angew. Chem.* **2017**, *56*, 3261.
[52] L. T. de Haan, C. Sanchez-Somolinos, C. M. Bastiaansen, A. P. Schenning, D. J. Broer, *Angew. Chem.* **2012**, *51*, 12469.
[53] C. D. Modes, K. Bhattacharya, M. Warner, *Phys. Rev. E* **2010**, *81*, 060701.
[54] S.-K. Ahn, T. H. Ware, K. M. Lee, V. P. Tondiglia, T. J. White, *Adv. Funct. Mater.* **2016**, *26*, 5819.
[55] L. T. de Haan, V. Gimenez-Pinto, A. Konya, T.-S. Nguyen, J. M. N. Verjans, C. Sánchez-Somolinos, J. V. Selinger, R. L. B. Selinger, D. J. Broer, A. P. H. J. Schenning, *Adv. Funct. Mater.* **2014**, *24*, 1251.
[56] M. Lahikainen, H. Zeng, A. Priimagi, *Nat. Commun.* **2018**, *9*, 4148.
[57] a) D. Liu, D. J. Broer, *Nat. Commun.* **2015**, *6*, 8334; b) D. Liu, C. W. M. Bastiaansen, J. M. J. den Toonder, D. J. Broer, *Macromolecules* **2012**, *45*, 8005; c) D. Liu, *Liq. Cryst.* **2016**, *43*, 2136.
[58] D. Liu, C. W. M. Bastiaansen, J. M. J. den Toonder, D. J. Broer, *Angew. Chem., Int. Ed.* **2012**, *51*, 892.
[59] D. Liu, D. J. Broer, *Angew. Chem., Int. Ed.* **2014**, *53*, 4542.
[60] D. Liu, L. Liu, P. R. Onck, D. J. Broer, *Proc. Natl. Acad. Sci. USA* **2015**, *112*, 3880.
[61] a) P. Beyer, E. M. Terentjev, R. Zentel, *Macromol. Rapid Commun.* **2007**, *28*, 1485; b) G. Maret, A. Blumstein, *Mol. Cryst. Liq. Cryst.* **1982**, *88*, 295.
[62] a) H. Zeng, P. Wasylczyk, D. S. Wiersma, A. Priimagi, *Adv. Mater.* **2018**, *30*, 1703554; b) S. Nocentini, C. Parmeggiani, D. Martella, D. S. Wiersma, *Adv. Opt. Mater.* **2018**, *6*, 1800207; c) M. P. da Cunha, Y. Foelen, R. J. H. van Raak, J. N. Murphy, T. A. P. Engels, M. G. Debije, A. P. H. J. Schenning, *Adv. Opt. Mater.* **2019**, *7*, 1801643.
[63] a) X. Lu, H. Zhang, G. Fei, B. Yu, X. Tong, H. Xia, Y. Zhao, *Adv. Mater.* **2018**, *30*, 1706597; b) M. P. da Cunha, S. Ambergen, M. G. Debije, E. F. G. A. Homburg, J. M. J. den Toonder, A. P. H. J. Schenning, *Adv. Sci.* **2020**, *7*, 1902842; c) M. Camacho-Lopez, H. Finkelmann, P. Palffy-Muhoray, M. Shelley, *Nat. Mater.* **2004**, *3*, 307.
[64] M. Yamada, M. Kondo, R. Miyasato, Y. Naka, J.-i. Mamiya, M. Kinoshita, A. Shishido, Y. Yu, C. J. Barrett, T. Ikeda, *J. Mater. Chem.* **2009**, *19*, 60.
[65] R. R. Kohlmeyer, J. Chen, *Angew. Chem.* **2013**, *52*, 9234.
[66] M. Rogóż, H. Zeng, C. Xuan, D. S. Wiersma, P. Wasylczyk, *Adv. Opt. Mater.* **2016**, *4*, 1689.
[67] H. Zeng, O. M. Wani, P. Wasylczyk, A. Priimagi, *Macromol. Rapid Commun.* **2018**, *39*, 1700224.
[68] H. Zeng, P. Wasylczyk, C. Parmeggiani, D. Martella, M. Burresi, D. S. Wiersma, *Adv. Mater.* **2015**, *27*, 3883.
[69] M. Yamada, M. Kondo, J. Mamiya, Y. Yu, M. Kinoshita, C. J. Barrett, T. Ikeda, *Angew. Chem.* **2008**, *47*, 4986.
[70] J. J. Wie, M. R. Shankar, T. J. White, *Nat. Commun.* **2016**, *7*, 13260.
[71] Y. C. Cheng, H. C. Lu, X. Lee, H. Zeng, A. Priimagi, *Adv. Mater.* **2020**, *32*, 1906233.
[72] H. Shahsavan, A. Aghakhani, H. Zeng, Y. Guo, Z. S. Davidson, A. Priimagi, M. Sitti, *Proc. Natl. Acad. Sci. USA* **2020**, *117*, 5125.
[73] H. Zeng, M. Lahikainen, L. Liu, Z. Ahmed, O. M. Wani, M. Wang, H. Yang, A. Priimagi, *Nat. Commun.* **2019**, *10*, 5057.
[74] T. J. White, N. V. Tabiryan, S. V. Serak, U. A. Hrozhyk, V. P. Tondiglia, H. Koerner, R. A. Vaia, T. J. Bunning, *Soft Matter* **2008**, *4*, 1796.
[75] S. Serak, N. Tabiryan, R. Vergara, T. J. White, R. A. Vaia, T. J. Bunning, *Soft Matter* **2010**, *6*, 779.
[76] K. M. Lee, M. L. Smith, H. Koerner, N. Tabiryan, R. A. Vaia, T. J. Bunning, T. J. White, *Adv. Funct. Mater.* **2011**, *21*, 2913.
[77] K. Kumar, C. Knie, D. Bleger, M. A. Peletier, H. Friedrich, S. Hecht, D. J. Broer, M. G. Debije, A. P. Schenning, *Nat. Commun.* **2016**, *7*, 11975.
[78] A. H. Gelebart, G. Vantomme, E. W. Meijer, D. J. Broer, *Adv. Mater.* **2017**, *29*, 1606712.
[79] R. Lan, J. Sun, C. Shen, R. Huang, Z. Zhang, L. Zhang, L. Wang, H. Yang, *Adv. Mater.* **2020**, *32*, 1906319.
[80] S. Palagi, A. G. Mark, S. Y. Reigh, K. Melde, T. Qiu, H. Zeng, C. Parmeggiani, D. Martella, A. Sanchez-Castillo, N. Kapernaum, F. Giesselmann, D. S. Wiersma, E. Lauga, P. Fischer, *Nat. Mater.* **2016**, *15*, 647.
[81] A. H. Gelebart, D. Jan Mulder, M. Varga, A. Konya, G. Vantomme, E. W. Meijer, R. L. B. Selinger, D. J. Broer, *Nature* **2017**, *546*, 632.

[82] O. M. Wani, R. Verpaalen, H. Zeng, A. Priimagi, A. P. H. J. Schenning, *Adv. Mater.* **2019**, *31*, 1805985.
[83] O. M. Wani, H. Zeng, A. Priimagi, *Nat. Commun.* **2017**, *8*, 15546.
[84] C. Li, Y. Liu, X. Huang, H. Jiang, *Adv. Funct. Mater.* **2012**, *22*, 5166.
[85] H. Zeng, O. M. Wani, P. Wasylczyk, R. Kaczmarek, A. Priimagi, *Adv. Mater.* **2017**, *29*, 1701814.
[86] M. P. da Cunha, H. S. Kandail, J. M. J. den Toonder, A. P. H. J. Schenning, *Proc. Natl. Acad. Sci. USA* **2020**, *117*, 17571.
[87] M. Prakash, D. Quere, J. W. Bush, *Science* **2008**, *320*, 931.
[88] M. Liu, S. Wang, L. Jiang, *Nat. Rev. Mater.* **2017**, *2*, 17036.
[89] C. Li, F. Cheng, J.-a. Lv, Y. Zhao, M. Liu, L. Jiang, Y. Yu, *Soft Matter* **2012**, *8*, 3730.
[90] Y. Zhan, J. Zhao, W. Liu, B. Yang, J. Wei, Y. Yu, *ACS Appl. Mater. Interfaces* **2015**, *7*, 25522.
[91] Y. Liu, C. Zhu, Y. Zhao, X. Qing, F. Wang, D. Deng, J. Wei, Y. Yu, *Adv. Mater. Interfaces* **2019**, *6*, 1901158.
[92] a) H. Zeng, H. Zhang, O. Ikkala, A. Priimagi, *Matter* **2020**, *2*, 194; b) M. Wang, S. M. Sayed, L.-X. Guo, B.-P. Lin, X.-Q. Zhang, Y. Sun, H. Yang, *Macromolecules* **2016**, *49*, 663.
[93] C. L. van Oosten, C. W. M. Bastiaansen, D. J. Broer, *Nat. Mater.* **2009**, *8*, 677.
[94] B. Zuo, M. Wang, B.-P. Lin, H. Yang, *Nat. Commun.* **2019**, *10*, 4539.
[95] B. Zuo, M. Wang, B.-P. Lin, H. Yang, *Chem. Mater.* **2018**, *30*, 8079.

Lang Qin is an associate researcher in the Department of Materials Science at Fudan University (China). He received his B.S. degree in Materials Chemistry from Sun Yat-sen University (China) in 2013 and his Ph.D. degree in Materials Physics and Chemistry from Fudan University (China) in 2018, where he continued his research as a postdoctoral research fellow for 2 years. His research interests focus on the design of functional liquid crystal materials and the construction of photonic crystals.

Xiaojun Liu is currently a Ph.D. student at the Department of Materials Science, Fudan University (China), where she received her M.S. degree in 2020. She received her B.S. degree in the Department of Materials Science and Engineering at South China University of Technology (China) in 2017. Her research interests focus on the construction of liquid crystal polymers and cholesteric liquid crystals.

Yanlei Yu is a professor in the Department of Materials Science at Fudan University, China. She graduated in Applied Chemistry from Anhui University in 1993 and obtained her M.S. degree in Polymer Chemistry and Physics from the University of Science and Technology of China in 1996. She gained her Ph.D. degree in Environmental Chemistry and Engineering from Tokyo Institute of Technology and was promoted to full professor at Fudan University in 2004. Her research interests focus on the development of photodeformable smart materials and light-controllable interface materials with photosensitive polymers and liquid crystal polymers.